PERGAMON

Chemical Engineering Science 54 (1999) 593–617

Chemical Engineering Science

Spatial effect of tumbling frequencies for motile bacteria on cell balance equations

Kevin C. Chen[a,1], Roseanne M. Ford[a,*], Peter T. Cummings[b,c]

[a] *Department of Chemical Engineering, University of Virginia, Charlottesville, VA 22903-2442, USA*
[b] *Department of Chemical Engineering, University of Tennessee, Knoxville, TN 37996-2200, USA*
[c] *Chemical Technology Division, Oak Ridge National Laboratory, Oak Ridge, TN 37381-6268, USA*

Received 3 December 1996; accepted 13 August 1998

Abstract

We performed dimensional reduction of Alt's three-dimensional cell balance equations to one-dimensional Segel's equations for an axisymmetrical case. The tumbling frequency of motile bacteria was assumed to switch between two different phases according to the sign of the perceived chemical gradients. Chemotactic bacteria responded to positive attractant gradients by suppressing the tumbling frequency, but appeared to be insensitive to negative attractant gradients. When both temporal and spatial attractant gradients were considered, this tumbling scenario constituted a limited swimming angle range. It was only within this angle range that the bacterial tumbling frequency was regulated according to the perceived attractant gradients. This angle range, characterized by the angle θ_0, plays a major role in determining the effective chemotactic responses. The bacterial density distribution in the velocity space was derived via a first-order perturbation analysis, and then applied to studies of two bacterial population transport parameters (the random motility coefficient and the chemotactic velocity). Two approaches different in dimensionality were presented. While the one-dimensional approach asymptotically yielded the expected, but incorrect, one-dimensional random motility coefficient as θ_0 approached zero, the three-dimensional approach always yielded the correct result. As to the chemotactic velocity, both approaches yielded the same expression. To validate our analyses and to explore possible limitations due to certain simplifying assumptions in the derivations, we further examined three numerical examples in which Galerkin finite element solutions of the Alt's three-dimensional equation were compared with analytical solutions. The agreement between the perturbation solutions and numerical solutions for all data over the entire range of θ_0 suggested that our perturbation analysis is valid under the condition of small constant attractant gradients. For chemical gradients of arbitrary magnitudes with temporal and spatial variations, our solutions were also found efficient and robust in comparison to numerical solutions.

Keywords: Chemotaxis; Cell balance equations; Perturbation theory; Motile bacteria

1. Introduction

In situ bioremediation (ISB) is a powerful, cost-effective method for restoring sites contaminated with hazardous organic chemicals by exploiting the natural degradative and migratory capability of bacteria (Madsen, 1991; Wilson *et al*., 1986). The overall degradation rate observed in the field is often limited by the rate at which the reactants and nutrients come in contact (i.e. mass transfer-limited) rather than by the rate of reaction as measured in a well-mixed laboratory reactor. Many of the bacterial species that are capable of transforming the pollutants into nontoxic products are also able to sense the location of the pollutants and move preferentially toward them (i.e. they exhibit chemotaxis). We have been interested for some time now in elucidating the role that chemotaxis plays in aiding the natural biological degradation of organic contaminants. Quantitative predictive tools for estimating the time and cost of an effective ISB strategy is often cited as a major obstacle to the broader adoption of ISB. The development of mathematical models that describe bacterial and contaminant transport is necessary for the design of ISB treatment technologies. Thus over the past few years mathematical quantification

* Corresponding author. Tel.: 001 804 924 7778; fax: 001 804 982 2658.
[1] Present address: Department of Physiology and Neuroscience, New York University Medical Center, 550 First Ave., New York, NY 10016, USA.

0009-2509/99/$ – see front matter
PII: S0009-2509(98)00268-1

of motile bacterial transport has emerged from conventional studies in chemical engineering (Ford *et al*., 1991; Frymier *et al*., 1994; Koster *et al*., 1993; Phillips *et al*., 1994; Rivero-Hudec and Lauffenburger, 1986; Staffeld *et al*., 1987).

Motile bacteria such as *Escherichia coli* propel themselves through surrounding fluid by rotating their flagella. When rotating in a counter-clockwise manner, the flagella form a twisted bundle propelling the bacterium forward in an approximately linear run that lasts on average about 1 s; when the flagella rotate in the clockwise direction, the bundle unravels and causes the bacterium to tumble in place for periods, which last about one-tenth of a second (Berg, 1988). After the tumble, as concluded by the resumed flagellar counter-clockwise rotation, the bacterium runs again with the next running direction randomly oriented. The random formation of the turn angle between the directions of one run and the next is usually described by a probability distribution known as the turn angle probability density distribution (Berg and Brown, 1972; Macnab and Koshland, 1972; Duffy and Ford, 1997). The experimentally measured turn angle probability density distribution for *E. coli* indicates a fairly weak correlation between runs. Thus, the motile bacterial movement is often viewed to be analogous to the random walks in molecular diffusion of gases (Berg, 1993).

Segel (1976, 1977) proposed a one-dimensional phenomenological model describing motile bacterial transport within a bulk aqueous phase. Rivero *et al*. (1989) and Ford *et al*. (1991) applied Segel's equations to interpret experimental data for the migration of a bacterial population under the influence of a one-dimensional chemical gradient. However, an important concern was how accurately a one-dimensional model can fit experimental data that result from three-dimensional random motion, even though, due to symmetry in the other two dimensions, the experimental setup and the extracted data seem suitable for a one-dimensional analysis. Ford and Cummings (1992) studied the cell balance equations proposed by Alt (1980) for N-dimensional bacterial motion, and suggested that under an axisymmetrical system the reduced one-dimensional bacterial swimming speed projected from three dimensional motion is $v/2$, where v represents the three-dimensional bacterial swimming speed. We (Chen *et al*., 1999) subsequently reanalyzed Alt's equations perturbatively and improved this conclusion by showing that the explicit forms of Segel's one-dimensional equations could be preserved if the one-dimensional swimming velocities in Segel's equations were replaced by a mean one-dimensional velocity, defined as the mean velocity weighted by the bacterial population distribution in the three-dimensional velocity space. The expression $v/2$ suggested by Ford and Cummings is merely the unperturbed result in the absence of spatial chemical gradients. Expanding the analysis of Ford and Cummings (1992), we (Chen *et al*., 1999) further discussed the appropriate forms of the random motility coefficient in terms of a system's dimensionality. In an earlier paper, Schnitzer (1993) studied random walk theories in arbitrary dimensions from a more general point of view. However, comparisons of similar quantities between systems in different dimensions were not addressed extensively. Brosilow *et al*. (1996) investigated the discretized form of Alt's equation and discussed the various forms of transport parameters that arose from different discretizations. Theoretically, for discretization of the velocity space into very large number of infinitesimal elements, Brosilow's results should reduce to those of Chen *et al*. (1999). Hence, the various geometrical factors associated with the transport parameters reported in Brosilow *et al*. (1996) are consequences of their coarse discretizations, and therefore are artifacts. However, an important result from their numerical calculations was that the Fickian fluxes in principal axes can be independently decoupled from each other in Alt's equation.

In those previous works, a smooth relationship between the mediated tumbling frequency and chemical gradients was employed. Here we presented an analysis for a *non-smooth* bacterial tumbling dependence on chemoattractant gradients based on observations from the tracking experiments performed by Berg and Brown (1972) and Macnab and Koshland (1972). Thus previous results based on smooth tumbling responses cannot be directly applied. By 'smooth' we mean that a function is both continuous in its zeroth- and first-order derivatives with respect to one of its independent variables. Berg and Brown (1972) found that some motile strains of *Escherichia coli* only respond to increasing chemoattractant concentrations or decreasing repellent concentrations. In other words, the tumbling frequency is only suppressed when a positive temporal gradient of attractants or a negative temporal gradient of repellents is sensed. In the converse situation, the tumbling frequency does not rise but remains at a basal value. The mathematical function describing the dependence of the tumbling frequency on the chemical gradient is non-smooth because the first derivative of the tumbling frequency with respect to the total chemical gradient is discontinuous at the point of zero gradient. This non-smooth scenario is different from what has been studied previously in which bacteria were assumed to follow a smooth dependence applicable to both positive and negative perceived chemical gradients. The macroscopic influence of this non-smooth tumbling response on bacterial transport and corresponding cell balance equations, although explored in a one-dimensional model (Rivero *et al*., 1989), has not yet been studied in three dimensions.

In this paper, we generalized our previous analytical approach to the non-smooth scenario in which bacteria only respond to positive attractant gradients. The analysis became more difficult because different tumbling

phases characterized by various swimming directions must now be separately considered for bacteria that are capable of random orientations. We not only theoretically investigated the possibility of dimensionally reducing Alt's three-dimensional cell balance equation to Segel's one-dimensional equations, but also explored the consequences of this non-smooth tumbling frequency on bacterial macroscopic transport parameters. The organization of this paper follows. We begin with a brief introduction of Alt's three-dimensional equations and review how they can be simplified and dimensionally reduced by invoking certain assumptions. Next in Section 3 we explore the one-dimensional analogy to Segel's phenomenological model by performing perturbative analyses on bacterial angular density solutions under the small one-dimensional attractant gradient. In Section 4 various macroscopic quantities of interest are explicitly integrated using the derived perturbative angular density solution from Section 3. Finally, the numerical experiments are provided as standard solutions to compare with analytical predictions as a verification of our perturbation theory and the corresponding results. To test possible limitations due to certain assumptions made in the analysis, a more general example of varying chemical gradients is also presented.

2. Three-dimensional Alt equations

Assuming each bacterium is represented as a random walker executing a piecewise linear path and by regarding tumbling and subsequent turning to be instantaneous, Alt's cell balance equations can be described by the following integro-differential system:

$$\frac{\partial \rho(\mathbf{r}, \hat{s}, \tau, t)}{\partial t} = -\frac{\partial \rho(\mathbf{r}, \hat{s}, \tau, t)}{\partial \tau} - \hat{s}\cdot \nabla_{\mathbf{r}}[v(\mathbf{r}, t)\,\rho(\mathbf{r}, \hat{s}, \tau, t)] - p_t(\mathbf{r}, \hat{s}, \tau, t)\,\rho(\mathbf{r}, \hat{s}, \tau, t) \tag{1a}$$

for $\tau > 0$, and

$$\rho(\mathbf{r}, \hat{s}, 0, t) = \int_0^\infty \int p_t(\mathbf{r}, \hat{s}', \tau, t)\,\rho(\mathbf{r}, \hat{s}', \tau, t) \times \kappa(\mathbf{r}, t, \hat{s}'; \hat{s})\,\mathrm{d}\hat{s}'\,\mathrm{d}\tau \tag{1b}$$

for $\tau = 0$.

Here $\rho(\mathbf{r}, \hat{s}, \tau, t)$ is the statistically expected bacterial number density at position $\mathbf{r}$, running in direction $\hat{s}$ (a unit vector) with a swimming speed $v(\mathbf{r}, t)$ and with a run time τ, $p_t(\mathbf{r}, \hat{s}, \tau, t)$ is the tumbling probability per unit time, often referred to as the tumbling frequency, and $\kappa(\mathbf{r}, t, \hat{s}'; \hat{s})$ is the turning probability density at $\mathbf{r}$ and t that a bacterium, given that the running direction was $\hat{s}'$ before tumbling, is running in the new direction $\hat{s}$ after tumbling. Regardless of the primes above $\hat{s}$, the first and the second directional arguments (either $\hat{s}'$ or $\hat{s}$) in $\kappa(\mathbf{r}, t, \hat{s}'; \hat{s})$ always denote the running direction before a tumble and that after a tumble, respectively.

Although Eqs. (1a) and (1b) are the most general forms, they are also difficult to solve. Fortunately, in many cases Eqs. (1a) and (1b) can be further simplified based on certain experimental observations. For instance, Ford and Cummings (1992) verified that by invoking the assumptions that (1) the probability of tumbling is independent of the run time τ and (2) κ is independent of $\mathbf{r}$ and t (both of which are consistent with experimental observations of biological systems), Alt's equations for the case possessing only a one-dimensional chemical gradient along z can be simplified, after applying axial symmetry to the z-axis, to become

$$\frac{\partial n(z, \theta, t)}{\partial t} = -\cos\theta\,\frac{\partial v(z, t) n(z, \theta, t)}{\partial z} - p_t(z, \theta, t) n(z, \theta, t) + \int_0^\pi p_t(z, \theta', t) n(z, \theta', t) K(\theta'; \theta) \sin\theta'\,\mathrm{d}\theta' \tag{2}$$

with the new bacterial angular density $n(z, \theta, t)$ as a function of z, t, and the running polar angle θ with respect to the positive z-axis. The $K(\theta'; \theta)$ in Eq. (2) was defined (Ford and Cummings, 1992) as a reduced turning probability density. $K(\theta'; \theta)$ represents the collected probability density that a single bacterium originally running in direction θ' before tumbling runs immediately into direction θ after tumbling. Similarly, the first and the second angle arguments in $K(\theta'; \theta)$ denote the swimming polar angles relative to the z-axis (the direction of chemical gradients) *before* and *after* a tumble, respectively. Based on the experimental observations of Berg and Brown (1972), we assume that when a bacterium randomly generates its next running direction $\hat{s}$, characterized by the spherical coordinates (θ, ϕ), the probability in the azimuthal angle ϕ^* measured from its previous running direction $\hat{s}'$, characterized by (θ', ϕ'), is uniform. However, the turn angle $\alpha[=\cos^{-1}(\hat{s}'\cdot\hat{s})]$ between those two successive runs is governed by a probability density function $W(\alpha)$ that satisfies $\int_0^\pi W(\alpha)\sin\alpha\,\mathrm{d}\alpha = 1$. Fig. 1 depicts the relative geometry and relationship between the fixed spherical coordinate system (θ, ϕ) based on the global z-axis and the local spherical coordinate system (α, ϕ^*) based on the previous running vector $\hat{s}'$. Performing a change of variables, $K(\theta'; \theta)$ can also be expressed as (Chen *et al.*, 1999)

$$K(\theta'; \theta) = -\frac{\int W(\alpha)\sin\alpha\,\mathrm{d}\phi^*(\alpha, \theta'; \theta)\,\mathrm{d}\alpha}{\pi\sin\theta\,\mathrm{d}\theta}. \tag{3}$$

It is implicitly assumed in Eq. (3) that the reduced turning probability density function $K(\theta'; \theta)$ represents a random process dependent only on the consecutive angles θ' and θ, resulting from the underlying assumption that $\kappa(\hat{s}'; \hat{s})$ is independent of time and position and is unaffected by chemical gradients.

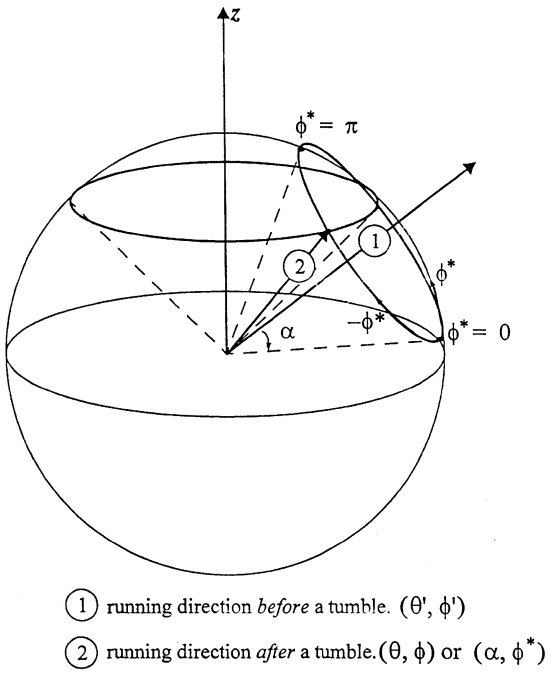

Fig. 1. Schematic diagram of the geometrical relationships between the global spherical coordinates (constructed by the global z-axis) and the local spherical coordinates (constructed by the running vector before a tumble).

From the corresponding coordinate transformation matrix, the following geometrical relationship should hold:

$$\cos\theta = -\sin\theta'\sin\alpha\cos\phi^* + \cos\theta'\cos\alpha, \tag{4}$$

which provides an implicit functional dependence between various angles. Note that in Eq. (4) the local spherical coordinates (α, ϕ^*) are defined according to the previous swimming direction (θ', ϕ'). This implicit dependence will become useful later in our analytical integration.

Because of technical difficulties in obtaining bacterial number distributions in the θ direction from experiments, we are interested in the experimentally accessible bacterial bulk density $c(z, t)$, a bulk variable by summing $n(z, \theta, t)$ over all swimming directions. Thus quantities independent of θ must be introduced first. The bacterial subpopulation densities, $n^{\pm}(z, t)$, were defined by Ford and Cummings (1992) according to the signs of the z-components of bacterial current running directions as

$$n^{+}(z, t) = \int_0^{\pi/2} n(z, \theta, t)\sin\theta\,\mathrm{d}\theta, \tag{5a}$$

$$n^{-}(z, t) = \int_{\pi/2}^{\pi} n(z, \theta, t)\sin\theta\,\mathrm{d}\theta. \tag{5b}$$

And the bulk bacterial density $c(z, t)$ and the net z-flux $J_z(z, t)$, assuming a constant swimming speed v hereafter, are respectively defined as

$$c(z, t) = \int_0^{\pi} n(z, \theta, t)\sin\theta\,\mathrm{d}\theta = n^{+}(z, t) + n^{-}(z, t). \tag{6a}$$

and

$$J_z(z, t) = v\int_0^{\pi} n(z, \theta, t)\cos\theta\sin\theta\,\mathrm{d}\theta. \tag{6b}$$

Ford and Cummings (1992) showed that Eq. (2) can be expressed in terms of the subpopulation densities by multiplying both sides by $\sin\theta\,\mathrm{d}\theta$ and integrating over θ:

$$\frac{\partial n^{+}(z, t)}{\partial t} = -\frac{\partial}{\partial z}v\int_0^{\pi/2}\sin\theta\cos\theta\cdot n(z, \theta, t)\,\mathrm{d}\theta - \underbrace{\int_0^{\pi/2} p_t(z, \theta, t)\,n(z, \theta, t)\left[1 - \int_0^{\pi/2} K(\theta; \theta')\sin\theta'\,\mathrm{d}\theta'\right]\sin\theta\,\mathrm{d}\theta}_{T.T.^{+}} + \underbrace{\int_{\pi/2}^{\pi} p_t(z, \theta', t)n(z, \theta', t)\left[\int_0^{\pi/2} K(\theta'; \theta)\sin\theta\,\mathrm{d}\theta\right]\sin\theta'\,\mathrm{d}\theta'}_{T.T.^{-}}, \tag{7a}$$

and

$$\frac{\partial n^{-}(z, t)}{\partial t} = -\frac{\partial}{\partial z}v\int_{\pi/2}^{\pi}\sin\theta\cos\theta\cdot n(z, \theta, t)\,\mathrm{d}\theta + \underbrace{\int_0^{\pi/2} p_t(z, \theta', t)n(z, \theta', t)\left[\int_{\pi/2}^{\pi} K(\theta'; \theta)\sin\theta\,\mathrm{d}\theta\right]\sin\theta'\,\mathrm{d}\theta'}_{T.T.^{+}} - \underbrace{\int_{\pi/2}^{\pi} p_t(z, \theta, t)n(z, \theta, t)\left[1 - \int_{\pi/2}^{\pi} K(\theta; \theta')\sin\theta'\,\mathrm{d}\theta'\right]\sin\theta\,\mathrm{d}\theta}_{T.T.^{-}}. \tag{7b}$$

Because the integration of the reduced turning probability density over all directions should be normalized, $\int_0^\pi K(\theta;\theta')\sin\theta'\,d\theta' = 1$ and the second terms on the right-hand side of both Eqs. (7a) and (7b) are equal, as are the last terms in both equations.

The purpose of defining such θ-independent variables (the bacterial subpopulation density quantities) is to draw an analogy to Segel's phenomenological equations (Segel, 1976, 1977), which assumed bacteria swam and turned only along the z-axis. However, successful elimination of θ from Eqs. (7a) and (7b) still depends on the *a priori* knowledge of the bacterial density distribution in θ. In general, such information as the cell density distribution in θ cannot be obtained elsewhere except from the original Eq. (2) itself. We will show in Section 3 how this information is extracted using a perturbation method. At present, our attention is rather directed to the task of simplifying Eqs. (7a) and (7b).

For comparison, the Segel's one-dimensional phenomenological cellular equations, after modification by Rivero *et al.* (1989), are shown below;

$$\frac{\partial n^+(z,t)}{\partial t} = -s\frac{\partial n^+(z,t)}{\partial z} - [p_t^+(z,t)n^+(z,t) - p_t^-(z,t)n^-(z,t)]p_r \quad (8a)$$

$$\frac{\partial n^-(z,t)}{\partial t} = s\frac{\partial n^-(z,t)}{\partial z} + [p_t^+(z,t)n^+(z,t) - p_t^-(z,t)n^-(z,t)]p_r, \quad (8b)$$

where s is the constant one-dimensional swimming speed, p_t^+ and p_t^- are the one-dimensional tumbling frequencies respectively in the positive and negative z directions, and p_r is the reversal probability defined by Rivero *et al.* (1989) to be $(1-\langle\cos\alpha\rangle)/2$, with $\langle\cos\alpha\rangle = \int_0^\pi \cos\alpha W(\alpha)\sin\alpha\,d\alpha$. Comparing Eqs. (8a) and (8b) with (7a) and (7b) reveals structural similarities, which motivate the equivalent definitions of the one-dimensional mean velocities, v_{1D}^+ and v_{1D}^-, in Eqs. (7a) and (7b) as

$$v_{1D}^+(z,t) = v\frac{\int_0^{\pi/2}\sin\theta\cos\theta\; n(z,\theta,t)\,d\theta}{n^+(z,t)}$$

and

$$v_{1D}^-(z,t) = -v\frac{\int_{\pi/2}^{\pi}\sin\theta\cos\theta\; n(z,\theta,t)\,d\theta}{n^-(z,t)}.$$

It can be seen that if the bacterial angular density distribution in θ is uniform, $n(z,\theta,t) = c(z,t)/2$, then $v_{1D}^+ = v_{1D}^- = v/2$, a conclusion drawn by Ford and Cummings (1992) for the isotropic case. It also can be verified that under the isotropic condition $\text{T.T.}^+ = \text{T.T.}^-$. Since anisotropy is the essential reason why chemotaxis happens, the application of the sole conclusion $v_{1D}^+ = v_{1D}^- = v/2$ drawn by Ford and Cummings is quite limited and can only be useful when combined with anisotropically perturbed results.

For the most general cases, if the last two lumped integral terms indicated by T.T.^+ and T.T.^- in Eqs. (7a) and (7b) can also be explicitly integrated and exactly manipulated as differences of two grouped quantities, each of them as a product of a mean tumbling frequency, a reversal probability, and the corresponding subpopulation density, then the analogy to Segel's equations exists. One goal of this paper is to directly show such an analogy, through which explicit definitions of the other two unknown quantities (the mean tumbling frequencies $p_t^\pm$ and the one-dimensional reversal probability p_r) can also be found. Note that the p_r introduced by Rivero *et al.* (1989) has not been proved to be appropriate in the case of a non-smoothly tumbling distribution function. However, the evaluation of the lumped integration terms is possible only when the bacterial number density distribution in the θ direction is available. Thus, we first find such a distribution using a perturbation technique to explicitly evaluate the integration terms. Before doing so, the angular dependence of $p_t(z,\theta,t)$ and $K(\theta';\theta)$ on the angle variable θ must be given. The relationship between $K(\theta';\theta)$ and the angles θ' and θ in terms of α and $W(\alpha)$ has been defined in Eqs. (3) and (4). As to the functional dependence of $p_t(z,\theta,t)$ on θ, we adopt the experimental observation in the tumbling response of *E. coli* (Berg and Brown, 1972) which is described below.

2.1. Biphasic tumbling frequency

Macnab and Koshland (1972) found that motile bacteria *Salmonella typhimurium* showed little response in the tumbling frequency when swimming down an attractant gradient. For some motile bacteria the tumbling frequency did not increase but remained at a basal level if the bacteria sensed a negative attractant gradient. Berg and Brown (1972) reported similar response behaviors for *E. coli* to chemoattractants and empirically found an exponential tumbling relationship with the positive attractant gradient. For this reason, Rivero *et al.* (1989) modified the single-phase exponential tumbling frequencies equation into a biphasic form in their one-dimensional model. They assumed that the exponential dependence of the tumbling frequency on attractant gradients proposed by Berg and Brown (1972) applied only when a swimming bacterium sensed a positive attractant gradient. This scenario describing the combined dependency of the tumbling frequency $p_t(z,\theta,t)$ on the swimming angle and chemical gradients can be rewritten in polar coordinates as

$$p_t(z,\theta,t) = \begin{cases} p_0\exp[-(\Gamma+\xi\cos\theta)] & \text{if } \Gamma+\xi\cos\theta \geqslant 0 \\ p_0 & \text{if } \Gamma+\xi\cos\theta < 0 \end{cases} \quad (9)$$

where p_0 is the basal tumbling frequency, Γ and ξ represent the temporal and spatial attractant gradients, respectively, and are defined as

$$\Gamma(z,t) = v\frac{\partial N_b}{\partial a}\frac{\partial a}{\partial t} \quad \text{and} \quad \xi(z,t) = v\frac{\partial N_b}{\partial a}\frac{\partial a}{\partial z}v$$

with N_b being the number of bound receptors per bacterium, a the attractant concentration, and v a scaling factor relating the chemical gradient and bacterial biological response. Note that Γ and ξ are the lumped parameters consisting of the chemical gradients, the biological scaling factor v, and the saturation effect $\partial N_b/\partial a$. The positive z-axis is set to be aligned in the direction of increasing attractant concentration. Therefore, ξ is positive for an attractant gradient and negative for a repellent gradient. We shall always assume $\xi \geqslant 0$ here, though the conclusions for $\xi < 0$ can also be easily extended from this analysis. The tumbling behavior described in Eq. (9), although continuous at the zero point $\Gamma + \xi\cos\theta = 0$, is *non-smooth* with respect to the total gradient at $\Gamma + \xi\cos\theta = 0$ as illustrated in Fig. 2.

It is emphasized that bacteria sense environmental changes only by means of temporal comparison of the status of the chemically bound receptors. This theory has been well demonstrated by the temporal-gradient experiments of Macnab and Koshland (1972) and Spudich and Koshland (1975). When a bacterium is swimming in a medium present with spatial chemical gradients, the increase or decrease of the chemical concentration around its surface receptors due to the swimming motion also causes bacteria to experience a temporal change in receptor status. Thus, the total chemical gradient sensed by bacteria should be the material derivative of chemical gradients, i.e. $\Gamma + \xi\cos\theta$. It is this anisotropic tumbling frequency, induced by the combined effect of bacterial locomotion and spatial chemical gradients, that results in the phenomenon of chemotactic migration. For the sake of convenience we still view the tumbling frequency p_t to be a function explicitly dependent on both the temporal and spatial chemical gradients. However, one should understand that the dependence on spatial chemical gradients is indirect and is a result of bacterial locomotion in spatially nonuniform environments.

When both temporal and spatial gradients are shallow, one can expand Eq. (9) by Taylor series about the zero point:

$$p_t(z,\theta,t) \simeq \begin{cases} p_0[1-(\Gamma+\xi\cos\theta)] & \text{if } \Gamma+\xi\cos\theta \geqslant 0 \\ p_0 & \text{if } \Gamma+\xi\cos\theta < 0. \end{cases} \quad (10)$$

One aspect to notice is that the analysis of the spatial influence of the *non-smooth* tumbling frequency on bacterial density distributions is meaningful only when Γ lies in the range $-\xi \leqslant \Gamma \leqslant \xi$. If $\Gamma > \xi \geqslant 0$, $\Gamma + \xi\cos\theta \geqslant 0$ in all swimming directions. The direction-dependent tumbling frequency thus applies everywhere, which is the case already studied by Chen *et al.* (1999). In contrast, if $\Gamma < -\xi \leqslant 0$, $\Gamma + \xi\cos\theta < 0$ and the tumbling frequency remains constant regardless of the swimming direction. In this case the existence of chemical gradients has no impact upon bacterial tumbling, and the bacterium behaves as if in an isotropic medium. To fully exploit the biphasic tumbling behaviors, we assume $-\xi \leqslant \Gamma \leqslant \xi$ so that $\Gamma + \xi\cos\theta$ may be positive, zero, or negative, depending on the direction the bacterium is swimming. Thus, there exists a limited angle range, in which p_t is dependent on θ, and out of which p_t remains constant. This limited angle range $[0, \theta_0]$ can be determined from

$$-1 \leqslant \cos\theta_0 = -\frac{\Gamma}{\xi} \leqslant 1, \quad (11)$$

where θ_0 is defined as the point where the total chemical gradient $\Gamma + \xi\cos\theta_0 = 0$. To keep $\cos\theta_0$ well-defined, we assume $|\Gamma|/\xi \leqslant 1$ and the order of magnitude for Γ is hence smaller than or equal to $O(\xi)$. For $|\Gamma|/\xi > 1$, θ_0 is set equal to π or zero according to its physical meaning: If $\Gamma > \xi > 0$ such that $\Gamma + \xi\cos\theta > 0$ for all $\theta \in [0, \pi]$, θ-dependent tumbling frequency applies to all directions and thus $\theta_0 = \pi$. By the same reasoning, $\theta_0 = 0$ if $\Gamma < -\xi < 0$.

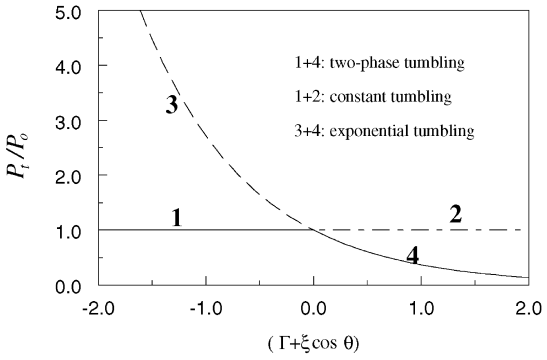

Fig. 2. Dimensionless tumbling frequency versus the total chemical gradients, designated as $\Gamma + \xi\cos\theta$, for different tumbling phases.

3. Density distribution in θ direction

In this section the bacterial density distribution in θ is studied via a perturbation analysis according to our previous procedures (Chen *et al.*, 1999). When there is no *spatial* attractant gradient, i.e. $\xi = 0$, the bacterial tumbling frequency is independent of θ and thus is isotropic in all swimming directions. Then the distribution of $n(z, \theta, t)$ in the θ direction becomes uniform (Schnitzer, 1993). When a weak spatial chemical gradient of magnitude ξ is suddenly imposed at time t_0, we assume that the uniformly distributed density profile can only be perturbed by

a small amount proportional to ξ. This is a reasonable hypothesis since now only the bacteria in the limited angle range respond to this gradient through the mediation of tumbling frequencies. Thus the bacterial angular density profile in θ will not vary significantly from uniformity for a sufficiently small ξ. The anisotropic density perturbation caused by this small parameter ξ can be studied by substituting the unperturbed solution $n(z, \theta, t_0) = c(z, t_0)/2$ as the initial condition and Eq. (10) for the linearized tumbling frequency into

$$n(z, \theta', t_0 + \Delta t) \simeq [1 - \Delta t\, p_t(z, \theta', t_0)]\, n(z, \theta', t_0) + \underbrace{\Delta t \int_{\theta_1}^{\theta_2} p_t(z, \theta, t_0)\, n(z, \theta, t_0)\, K(\theta; \theta') \sin\theta \, \mathrm{d}\theta}_{I}, \tag{12}$$

which is derived from Eq. (2) by neglecting the convective term. That is, we are only interested in the changes of bacterial density distribution in θ caused by the anisotropic tumbling frequency. Neglecting the convection term is justifiable provided that the dimensionless group $v/(zp_t)$ is smaller than unity. The physical meaning is that as long as the smallest distance z over which there exists a significant bacterial density variation is larger than the convection distance characterized by the multiplication of the swimming speed v and the mean run time $1/p_t$, the change of bacterial concentration resulting from the convection term during an extremely short interval $\Delta t (\ll 1/p_t)$ is negligible. This criterion can be justified for *E. coli* as an example by assuming the swimming speed to be 30 μm/s and the mean run time to be 1 second, which results in a critical distance of 3×10^{-3} cm. In most cases the smallest distance over which bacterial density varies significantly can be safely assumed to be larger than this value. Thus, use of Eq. (12) for a short time period to study the cellular orientation density distribution is appropriate. Notice that in Eq. (12) the unprimed θ now denotes the swimming angle *before* a tumble, and the primed θ' denotes the swimming angle *after* a tumble.

A direct interpretation of Eq. (12) is that the bacterial density $n(z, \theta', t_0 + \Delta t)$ swimming in θ' at time $t_0 + \Delta t$ is composed of those that swam in θ' at t_0 and remain at θ' at $t_0 + \Delta t$ not tumbling, and of those that swam in all directions (including θ') at t_0 and change via tumbling into the angle θ' at $t_0 + \Delta t$. The valid integration range for θ in Eq. (12) for a fixed θ' and α, instead of being $[0, \pi]$, should be $[\theta_1, \theta_2]$ (Chen *et al.*, 1999) and is given by

$$|\theta' - \alpha| = \theta_1 \leqslant \theta \leqslant \theta_2 = \begin{cases} \theta' + \alpha & \text{if } \theta' + \alpha \leqslant \pi \\ 2\pi - (\theta' + \alpha) & \text{if } \theta' + \alpha > \pi. \end{cases} \tag{13}$$

Using Eq. (3) for $K(\theta; \theta')$ and Eq. (4) to calculate $\partial\theta'/\partial\phi^*$, the integral I in Eq. (12) becomes

$$I = \frac{c(z, t_0)}{2\pi} \int_0^{\pi} W(\alpha) \underbrace{\left[\int_{\theta_1}^{\theta_2} \frac{p_t(z, \theta, t_0)}{\sin\phi^*(\alpha, \theta)} \mathrm{d}\theta \right]}_{Y} \mathrm{d}\alpha. \tag{14}$$

Let us denote the integration within the squared brackets Y. The outcome of this integral Y varies according to the phase of p_t determined by the relative location of the dividing angle θ_0 in $[\theta_1, \theta_2]$. Depending on the location of θ_0, the θ-integral, Y, can be analyzed from the following three different situations:

(1) If both the integration limits θ_1 and θ_2 are within the *direction-independent* region, i.e., $[\theta_1, \theta_2] \cap [0, \theta_0] = \{0\}$, the integral should be performed with $p_t = p_0$. Applying our previous results (Chen *et al.*, 1999), the squared integral Y in Eq. (14) simplifies to $Y/(p_0 \sin\alpha) = \pi$.

(2) If θ_0 is inside the integration range, i.e. $[0, \theta_0] \subset [\theta_1, \theta_2]$, the integral should be split into two parts: one with a θ-dependent tumbling frequency and one with a constant tumbling frequency. Upon utilizing Eq. (4) for $\sin\phi^*$, we obtain

$$\begin{aligned} Y &= p_0 \int_{\theta_1}^{\theta_0} \frac{1 - (\Gamma + \xi\cos\theta)}{\sin\phi^*(\alpha, \theta)} \mathrm{d}\theta + p_0 \int_{\theta_0}^{\theta_2} \frac{1}{\sin\phi^*(\alpha, \theta)} \mathrm{d}\theta \\ &= p_0 \pi \sin\alpha + p_0 \sin\alpha \cdot (\Gamma + \xi\cos\alpha\cos\theta') \\ &\quad \times \sin^{-1}\left(\frac{\cos\theta - \cos\alpha\cos\theta'}{\sin\alpha\sin\theta'} \right)\Bigg|_{\theta_1}^{\theta_0} - p_0 \xi \sin\alpha \\ &\quad \times \sqrt{\sin^2\alpha\sin^2\theta' - (\cos\theta - \cos\alpha\cos\theta')^2}\,\Bigg|_{\theta_1}^{\theta_0}. \end{aligned} \tag{15}$$

Further simplification of Eq. (15) is possible only if we define another azimuthal angle $\phi_0^*(\alpha, \theta_0)$ corresponding to θ_0 according to Eq. (4),

$$\cos\theta_0 = -\sin\theta'\sin\alpha\cos\phi_0^* + \cos\theta'\cos\alpha. \tag{16}$$

Upon using Eq. (16), the arcsine of the second term and the squared root of the last term in Eq. (15) are simplified and Eq. (15) becomes

$$\begin{aligned} \frac{Y}{p_0 \sin\alpha} &= \pi(1 - \Gamma - \xi\cos\alpha\cos\theta') \\ &\quad + \phi_0^*(\Gamma + \xi\cos\alpha\cos\theta') \\ &\quad - \xi\sin\alpha\sin\theta'\sin\phi_0^*. \end{aligned} \tag{17}$$

It is seen that if $\phi_0^* = \pi$, Eq. (17) reduces to the result of (1); If $\phi_0^* = 0$, it reduces to Eq. (18) below.

(3) If the integration limits θ_1 to θ_2 are within the *direction-dependent* region, i.e. $[\theta_1, \theta_2] \subseteq [0, \theta_0]$,

then the integral should be calculated with $p_t \simeq p_0(1 - \Gamma - \xi\cos\theta)$ and yields (Chen *et al.*, 1999)

$$\frac{Y}{p_0 \sin\alpha} = \pi(1 - \Gamma - \xi\cos\alpha\cos\theta'). \tag{18}$$

Thus depending on the location of the dividing angle θ_0 relative to the integration limits θ_1 and θ_2, three distinct expressions for Y are produced. For detailed derivations regarding the integration procedure, see Chen (1997).

The integral Y represents the probability that a bacterium originally swimming in all possible directions tumbles and turns with the turn angle α into the desired direction θ'. One should add up all such probabilities by allowing the turn angle α to change freely from 0 to π. That is, one needs to integrate the integral I in Eq. (14) over α. Two difficulties will be encountered. First, the appropriate expression for Y directly depends on the location of θ_0 and the span of the integration range θ_1 to θ_2. Second, $\phi_0^*(\alpha)$ is an implicit function of α as well. We can think of the integration range $[\theta_1, \theta_2]$ in an alternative fashion by regarding the direction θ' as a centered axis in the range, and then expanding an angle α on both sides of the θ'-axis, as defined by Eq. (13). Thus the spanning degree of α from the θ'-axis determines the integration limits θ_1 and θ_2, and consequently determines the appropriate expression for Y, depending on whether or not θ_0 is included in the integration range and, if so, on which side of the range it is. We need to consider all possible geometries for the relative locations of θ_0 and the centered axis θ' with the expanded angle α. From Fig. 3 it shows geometrically that when the turn angle α, centered at θ', expands from 0 to π, two basic scenarios can be identified. One is when the integration range $[\theta_1, \theta_2]$, centered at θ', does not include the angle θ_0, and the other is when it does. Considering all possible conditions, the integration over α in Eq. (14) should be the consecutive summation of the three separate integrals in $[0, \alpha_1)$, $[\alpha_1, \alpha_2]$, and $(\alpha_2, \pi]$. The angles α_1 and α_2

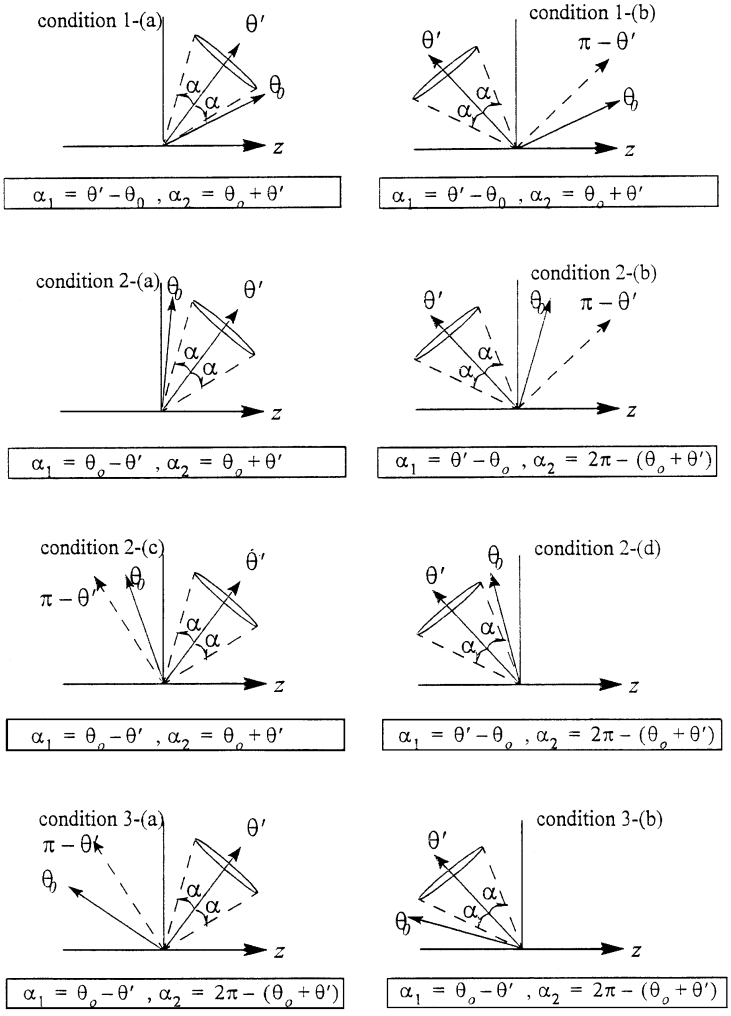

Fig. 3. Geometrical relationships between θ' and θ_0.

separating integrals adjacent to each other are similarly given by

$$\alpha_1 = |\theta' - \theta_0| \quad \text{and}$$

$$\alpha_2 = \begin{cases} \theta' + \theta_0 & \text{if } \theta' + \theta_0 \leqslant \pi \\ 2\pi - (\theta' + \theta_0) & \text{if } \theta' + \theta_0 > \pi. \end{cases}$$

For each integral, the appropriate choice for Y, depending on the relative location of θ_0 to the integration limits θ_1 and θ_2, should be one of the three expressions in the situations (1), (2), and (3) described above. Taking the conditions 3-(a) and 3-(b) in Fig. 3 as an example, the integral I should be the sum of the three consecutive integrals that, in sequence, adopt the results in situations (3), (2), and (3). Therefore, the α-integration given in Eq. (14) for conditions 3-(a) and 3-(b) should be

$$I = \frac{cp_0}{2\pi}\left\{\pi\int_0^{\alpha_1} W(\alpha)\sin\alpha\,[1 - \Gamma - \xi\cos\alpha\cos\theta']\,\mathrm{d}\alpha + \int_{\alpha_1}^{\alpha_2} W(\alpha)\sin\alpha\begin{bmatrix}\pi(1 - \Gamma - \xi\cos\alpha\cos\theta') \\ +\,\phi_0^*(\Gamma + \xi\cos\alpha\cos\theta') \\ -\,\xi\sin\alpha\sin\theta'\sin\phi_0^*\end{bmatrix}\mathrm{d}\alpha + \pi\int_{\alpha_2}^{\pi} W(\alpha)\sin\alpha[1 - \Gamma - \xi\cos\alpha\cos\theta']\,\mathrm{d}\alpha\right\}. \quad (19)$$

Similarly, the integral I for other conditions depicted in Fig. 3 can also be obtained as combinations of the three situations in different sequences. To integrate the three regional integrals in Eq. (19) to yield more explicit expressions, the turn angle probability density function $W(\alpha)$ must be defined. However, this piece of information could have been spared if a smooth tumbling frequency was assumed (Chen *et al.*, 1999). For a smooth tumbling frequency, $\theta_0 = \pi$, which means of all conditions in Fig. 3, only the conditions 3-(a) and 3-(b) apply. Then in Eq. (19) the regional integral over $[\alpha_1, \alpha_2]$ disappears since $\alpha_1 = \alpha_2 = \pi - \theta'$. The other two integration regions can therefore be combined together yielding a continuous α-integration from 0 to π and reducing Eq. (19) to

$$I = \frac{cp_0}{2}[1 - \Gamma - \xi\langle\cos\alpha\rangle\cos\theta'].$$

This is the same result as derived in our previous paper (Chen *et al.*, 1999) in which a smooth tumbling frequency was employed. Currently, we are unable to integrate I without knowing $W(\alpha)$ specifically. For illustration purposes, we chose the simplest case that $W(\alpha)$ is uniformly distributed, $W(\alpha) = 1/2$, meaning that the bacterial turning behavior exhibits no directional persistence, $\langle\cos\alpha\rangle = 0$.

The two integrals over $[0, \alpha_1)$ and $(\alpha_2, \pi]$ can be obtained easily since Γ, ξ, and θ' are all independent of α. Nevertheless, the integral over $[\alpha_1, \alpha_2]$ involving $\phi_0^*(\alpha, \theta_0)$ as a complex function for fixed θ_0 and θ' is formidable. We carried out the derivations and included only key steps of the integration over $[\alpha_1, \alpha_2]$, assuming $W(\alpha) = 1/2$, in the appendix. The derived results for each condition in Fig. 3 were then substituted into Eq. (12). After rearrangement and classification, the perturbative angular density solution at $t_0 + \Delta t$, as ξ and Γ were imposed at t_0, is eventually reduced to the fairly simple representations,

$$n(z, \theta', t_0 + \Delta t) = \frac{c}{2}\left\{1 - \Delta t p_0\left(\frac{1 - \cos\theta_0}{2}\right)\left(\Gamma + \frac{\xi}{2}(1 + \cos\theta_0)\right)\right\},$$

… for conditions 1(a), (b) and 2(b), (d) (20a)

$$n(z, \theta', t_0 + \Delta t) = \frac{c}{2}\left\{1 - \Delta t p_0\left[\left(\frac{1 - \cos\theta_0}{2}\right)\left(\Gamma + \frac{\xi}{2}(1 + \cos\theta_0)\right) - (\Gamma + \xi\cos\theta')\right]\right\},$$

… for conditions 2(a), (c) and 3(a), (b). (20b)

The perturbative density solutions together with the uniform (unperturbed) solution are plotted in Fig. 4 in polar coordinates. One can see that the uniformly distributed density profile is still preserved in the region $[\theta_0, \pi]$, with a uniform density decrease in compensation for the density increases in the region $[0, \theta_0]$. The density profile in $[0, \theta_0]$ is deformed most in directions of increasing attractant concentrations due to the aggregation of bacteria induced by the reduced tumbling frequencies in this range. It is this convex density distribution that contributes to the biased migration of bacterial populations (chemotaxis). The extent of deformation, according to Eqs. (20a) and (20b), depends on the strength of chemical gradients Γ and ξ, and the basal tumbling frequency p_0.

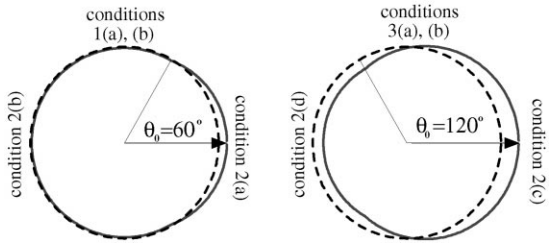

Fig. 4. The perturbed (solid curves) and unperturbed (dashed curves) bacterial density distribution functions in spherical polar coordinates for $\theta_0 = 60^\circ$ and $\theta_0 = 120^\circ$.

3.1. Perturbation analysis

Based upon the perturbative representations of the density solution at $t_0 + \Delta t$ given above, we postulate the perturbative expansions for the density $n(z, \theta, t; \xi)$ as

$$n(z,\theta,t;\xi)=\begin{cases}\dfrac{c(z,t)}{2}[1-n_0(z,t;\xi)+n_s(z,t)(\Gamma+\xi\cos\theta)]+O(\xi^2\cos^2\theta), & \theta\leqslant\theta_0\\ \dfrac{c(z,t)}{2}[1-n_0(z,t;\xi)]+O(\xi^2\cos^2\theta), & \theta>\theta_0\end{cases} \tag{21}$$

where $n_0(z, t; \xi)$ and $n_s(z, t)$ are the perturbation expansion coefficients for $n(z, \theta, t; \xi)$. Note that n_0 has an order of magnitude $O(\xi)$, but n_s is of $O(1)$ because of the prior separation of the factor $(\Gamma + \xi \cos\theta)$ from n_s. Hereafter we also explicitly include ξ as an independent parameter affecting bacterial density distribution in θ.

Substituting Eq. (21) for the bacterial density distribution and Eq. (10) for the tumbling frequencies back into Eq. (2) and equating to zero the coefficients of successive powers of ξ^0 and ξ^1 yields a set of coupled partial differential equations (PDEs) for n_0 and n_s. They can be solved to yield

$$n_0(z,t;\xi)=\mathscr{K}\cdot n_s(z,t;\xi)=\frac{\mathscr{K}}{\mathscr{K}+1}\{1-\mathrm{e}^{-p_0\int_{t_0}^{t}(\mathscr{K}+1)Dt'}\}. \tag{22}$$

Here $\mathscr{K}$ represents the ratio of n_0 and n_s and is given as

$$\mathscr{K}=\left(\frac{1-\cos\theta_0}{2}\right)\left[\Gamma+\frac{\xi}{2}(1+\cos\theta_0)\right], \tag{23}$$

which is of the order $O(\xi)$, consistent with our previous formulation about the orders of n_0 and n_s. The integral notation Dt' in the exponent is meant to indicate that the integration is carried out along the Lagrangian path $Dt' \equiv \partial t + v\hat{s}\cdot\nabla$. For a very short period of time Δt right after t_0, Eq. (22) is approximated to give $n_0 \simeq \Delta t p_0 \dfrac{1-\cos\theta_0}{2}[\Gamma + (\xi/2)(1+\cos\theta_0)]$, and $n_s \simeq \Delta t p_0$. Substituting these short-time representations back into Eq. (21) yields the one-step perturbative density distributions Eqs. (20a) and (20b), thus confirming the postulated perturbative forms.

4. Analogy to Segel's 1-d equations

After the perturbative expressions for $n(z, \theta, t; \xi)$ are verified, other macroscopic quantities of interest can be explicitly evaluated in terms of this perturbative distribution. Bear in mind that $\theta_0 = \theta_0(z, t)$, i.e., θ_0 is a function of space and time since the point at which $\Gamma + \xi\cos\theta_0 = 0$ depends on both Γ and ξ which vary with z and t. It is again necessary to consider two different situations, $\theta_0 \in [0, \pi/2]$ and $\theta_0 \in [\pi/2, \pi]$. Hereafter the notation u_0 is used to indicate $\cos\theta_0$ for simplicity. We also simplify the final results by replacing Γ with $-\xi u_0$ and n_0 with $n_s\mathscr{K}$, using the relationship, $n_0 = n_s\mathscr{K} = n_s\xi(1-u_0)^2/4$, from Eq. (23).

Type 1: $\theta_0 \in [0, \pi/2]$. Due to space limitation, detailed derivations of the θ-integration involved in various macroscopic quantities will not be provided below (for details see Chen, 1997). Instead, we suggest readers verify these expressions by examining their corresponding limiting situations.

For the case $\theta_0 \in [0, \pi/2]$, $n^+(z, t; \xi)$ and $n^-(z, t; \xi)$ from their definitions are found to be

$$n^{\pm}(z,t;\xi)=\frac{c}{2}\left\{1\pm n_s\frac{\xi}{4}(1-u_0)^2\right\}+O(\xi^2). \tag{24}$$

Then the conservation requirement for the bulk density $c(z, t; \xi) = n^+ + n^-$ is automatically satisfied. Note that the truncated terms $O(\xi^2)$ in Eq. (24) should have opposite signs in n^+ and n^-. However, our analysis based on a first-order perturbation can not confirm this without carrying out the analysis to the next order. Further, if p_t remains constant either due to the zero spatial chemical gradient ($\xi = 0$) or the zero dividing angel ($u_0 = 1$), the perturbation term associated with n_s vanishes and the unperturbed solution, $n^+ = n^- = c/2$, is recovered. The lumped tumbling terms in Eqs. (7a) and (7b) are also evaluated explicitly,

$$\mathrm{T.T.}^+ - \mathrm{T.T.}^- = -p_0\frac{c}{2}\left\{1-n_s\left[1+\frac{\xi}{4}(1-u_0)^2\right]\right\}\times\frac{(1-u_0)^2}{4}\xi+O(\xi^2). \tag{25}$$

As mentioned previously, the unperturbed solution is rendered when $\xi = 0$ or $u_0 = 1$, indicating that $\mathrm{T.T.}^+ - \mathrm{T.T.}^-$ should be zero as expected under the same conditions. If the mean tumbling frequencies $\tilde{p}_t^+$ and $\tilde{p}_t^-$ respectively associated with the positive moving bacteria and the negative moving bacteria are defined to be the integrals of the biphasic p_t times $\sin\theta\,\mathrm{d}\theta$ over $[0, \pi/2]$ and $[\pi/2, \pi]$, respectively, i.e.

$$\tilde{p}t^+ = \int_0^{\theta_0} p_0(1-\Gamma-\xi\cos\theta)\sin\theta\,\mathrm{d}\theta + \int_{\theta_0}^{\pi/2} p_0\sin\theta\,\mathrm{d}\theta = p_0\left\{1-\frac{\xi}{2}(1-u_0)^2\right\} \tag{26a}$$

and

$$\tilde{p}_t^- = \int_{\pi/2}^{\pi} p_0 \sin\theta \, \mathrm{d}\theta = p_0 \tag{26b}$$

we find that the leading term of $\tilde{p}_t^+ n^+ - \tilde{p}_t^- n^-$,

$$\tilde{p}_t^+ n^+ - \tilde{p}_t^- n^- = -\, p_0 \frac{c}{2}\left\{1 - n_s\left[1 + \frac{\xi}{4}(1-u_0)^2\right]\right\} \times \frac{(1-u_0)^2}{2}\xi + O(\xi^2) \tag{27}$$

can be matched with the leading term of Eq. (25) after multiplying Eq. (27) by a numerical factor 1/2. Since $W(\alpha) = 1/2$ indicates no directional persistence, it seems a natural choice that we define a reversal probability $p_r = 1/2$ so that Eq. (25) can be written as

$$\mathrm{T.T.}^+ - \mathrm{T.T.}^- = (\tilde{p}_t^+ n^+ - \tilde{p}_t^- n^-) p_r + O(\xi^2). \tag{28}$$

Type 2: $\theta_0 \in [\pi/2, \pi]$. Following a similar procedure, we may obtain the following subpopulation quantities for $\theta_0 \in [\pi/2, \pi]$,

$$n^{\pm}(z, t; \xi) = \frac{c}{2}\left\{1 \pm n_s \frac{\xi}{4}(1 - 2u_0 - u_0^2)\right\} + O(\xi^2). \tag{29}$$

It is once again confirmed that the bulk density $c(z, t; \xi)$ is conserved by the sum of $n^+(z, t; \xi)$ and $n^-(z, t; \xi)$. Eq. (29) is also found to be smoothly and continuously matched with Eq. (24) at $\theta_0 = \pi/2$: For the case $\theta_0 = \pi$ ($u_0 = -1$), Eq. (29) recovers back the results of our previous paper (Chen *et al.*, 1999) in which a smooth function for the tumbling frequency was studied. We also have the following expression for the difference of the two lumped tumbling terms,

$$\mathrm{T.T.}^+ - \mathrm{T.T.}^- = -\, p_0 \frac{c}{2}\left\{1 - n_s\left[1 + \frac{\xi}{4}(1-u_0)^2\right]\right\} \times \frac{1 - 2u_0 - u_0^2}{4}\xi + O(\xi^2). \tag{30}$$

At $u_0 = -1$, Eq. (30) also reduces back to our previous result for $\mathrm{T.T.}^+ - \mathrm{T.T.}^-$ based on the smooth tumbling frequency. Likewise, if the mean tumbling frequencies are defined as the surface integrals of p_t over the corresponding hemispherical surfaces in the velocity space by

$$\tilde{p}_t^+ = \int_0^{\pi/2} p_0(1 - \Gamma - \xi\cos\theta)\sin\theta \, \mathrm{d}\theta = p_0\left\{1 - \frac{\xi}{2}(1 - 2u_0)\right\} \tag{31a}$$

and

$$\tilde{p}_t^- = \int_{\pi/2}^{\theta_0} p_0(1 - \Gamma - \xi\cos\theta)\sin\theta \, \mathrm{d}\theta + \int_{\theta_0}^{\pi} p_0 \sin\theta \, \mathrm{d}\theta = p_0\left(1 - \frac{\xi}{2}u_0^2\right) \tag{31b}$$

then one also finds the leading-term match,

$$\tilde{p}_t^+ n^+ - \tilde{p}_t^- n^- = -\, p_0 \frac{c}{2}\left\{1 - n_s\left[1 + \frac{\xi}{4}(1-u_0)^2\right]\right\} \times \frac{1 - 2u_0 - u_0^2}{2}\xi + O(\xi^2) \tag{32}$$

with $\mathrm{T.T.}^+ - \mathrm{T.T.}^-$ in Eq. (30), provided that $(\tilde{p}_t^+ n^+ - \tilde{p}_t^- n^-)$ is multiplied by the same factor $p_r = 1/2$. Finally, it is easy to verify that all the macroscopic expressions derived from the two hemispherical regions are smoothly matched at the junction $\theta_0 = \pi/2$. The perturbative v_{1D}^+ and v_{1D}^- also can be obtained, though we will not show their explicit expressions here.

Thus, by retaining only terms of zeroth and first orders of ξ, we showed that Alt's three-dimensional cell balance equation Eq. (2) can be cast into the same forms as Segel's one-dimensional phenomenological equations,

$$\frac{\partial n^+(z,t)}{\partial t} = -\frac{\partial [v_{1D}^+ n^+(z,t)]}{\partial z} - [\tilde{p}_t^+(z,t) n^+(z,t) - \tilde{p}_t^-(z,t) n^-(z,t)] p_r \tag{33a}$$

$$\frac{\partial n^-(z,t)}{\partial t} = \frac{\partial [v_{1D}^- n^-(z,t)]}{\partial z} + [\tilde{p}_t^+(z,t) n^+(z,t) - \tilde{p}_t^-(z,t) n^-(z,t)] p_r \tag{33b}$$

with a slight modification in the newly-defined one-dimensional convective velocities v_{1D}^+ and v_{1D}^-. One can easily see that the definition of the one-dimensional mean tumbling frequencies is the crucial key to accomplishing the leading-term matches between the difference of the lumped tumbling terms $\mathrm{T.T.}^+ - \mathrm{T.T.}^-$ and the product of our desired quantity, $(\tilde{p}_t^+ n^+ - \tilde{p}_t^- n^-) p_r$. This is because physically n^+ and n^- (also the variables c and J_z) allow no alternative definitions, whereas the mean tumbling frequency, a collective term, can be manipulated. The definition of $\tilde{p}_t^{\pm}$ is based on the biphasic p_t linearly expanded with respect to small chemical gradients. Here we propose other definitions for the mean tumbling frequencies, which are not theoretically based but appear to be more general,

$$\tilde{p}_t^+ = p_0 \exp\left[-\int_{[0,\pi/2]\cap[0,\theta_0]} (\Gamma + \xi\cos\theta)\sin\theta \, \mathrm{d}\theta\right] \tag{34a}$$

and

$$\tilde{p}_t^- = p_0 \exp\left[-\int_{[\pi/2,\pi]\cap[0,\theta_0]} (\Gamma + \xi\cos\theta)\sin\theta \, \mathrm{d}\theta\right] \tag{34b}$$

for arbitrary values of Γ and ξ. It can be seen that Eqs. (34a) and (34b), respectively, reduce to Eqs. (26a) and (26b) or Eqs. (31a) and (31b), depending on the location of θ_0, when Γ and ξ are far less than one. However, Eqs. (34a) and (34b) always ensure *positive definite* $\tilde{p}_t^+$ and $\tilde{p}_t^-$ at large chemical gradients. We will

show in the numerical section that follows that incorporating Eqs. (34a) and (34b) in the theoretical analysis still yields quite close predictions to the numerical solutions solved from Eq. (2).

5. Fickian expressions

Although we have shown that for motile bacteria obeying a non-smooth tumbling frequency the correspondent three-dimensional cell balance equation can be cast into the same forms as the one-dimensional Segel's equations Eqs. (8a) and (8b), the influence of this non-smooth tumbling frequency on macroscopic transport behavior is still unclear. At the macroscopic level, the experimentally accessible variable $c(z, t; \xi)$ is conventionally predicted from the mass conservation equation,

$$\frac{\partial c}{\partial t} = -\frac{\partial J_z}{\partial z} \tag{35a}$$

upon adopting a constitutive flux relation,

$$J_z = -\frac{\partial}{\partial z}(\mu c) + V_c\, c. \tag{35b}$$

Here μ, analogous to molecular diffusivity, is called the random motility coefficient; and V_c, analogous to bulk convective velocity, is called chemotactic velocity. Next we proceed to pursue analytical expressions for these two macroscopic transport parameters.

Two distinct approaches differing in dimensionality were adopted. One is to directly integrate the cell balance equations (2) by $d(\cos\theta)$ and $\cos\theta\, d(\cos\theta)$ over $[-1, 1]$ to yield Eq. (35a) and a transient PDE for Eq. (35b), respectively. This approach has been exemplified by Schnitzer (1993) and will be shown later to yield correct expressions for μ for three-dimensional random walks. In another approach we directly applied Segel's one-dimensional approach to Eqs. (33a) and (33b). That is, Eqs. (33a) and (33b), as the integral results from Eq. (2), were treated as two *one-dimensional* phenomenological subpopulation equations instead of those derived from axial simplifications of the three-dimensional equation. In a previous paper (Chen *et al.*, 1999) we found that μ and V_c resulting from the three-dimensional approach by angular integration are the same as those from the Segel's one-dimensional approach. This consistency is attributed to the use of a smooth tumbling frequency, which also leads to a smooth angular density distribution. In this paper, however, the distribution of $n(z, \theta, t; \xi)$ is non-smooth at the angle θ_0, which results from adopting a non-smooth tumbling frequency. We believe this non-smoothness accounts for the possible discrepancies between the explicit expressions of μ in the two approaches. The reason we include the Segel's one-dimensional approach here is because Segel's approach has been so popular in the past that many researchers are accustomed to directly applying the results to their systems regardless of the intrinsic dimensionality restraint (Rivero *et al.*, 1989; Ford *et al.*, 1991; Lapidus *et al.*, 1976; Staffeld *et al.*, 1987; Widman *et al.*, 1997). Chen (1997) noted that although the functional structure of the net flux expression derived from Segel's results is generically similar to that of a three-dimensional result, the geometrical factors resulting from systems of different dimensionality are distinct. A consequence of misusing Segel's one-dimensional model in quantifying bacterial biased migrations that result from three-dimensional random motion is the inclusion of extraneous geometrical factors in the cellular biological parameters, such as the random motility and chemotactic velocity. A study of such geometrical factors will help clarify the true biological parameters measured in experiments.

5.1. Segel's one-dimensional approach

We showed earlier that Segel's one-dimensional subpopulation equations can be recovered from Alt's equations in the context of a first-order perturbation theory. To extend our analysis and derive expressions for the equilibrium cellular flux, we use the following procedure: adding Eqs. (33a) and (33b) together and subtracting one from the other, followed by replacing $(n^+ - n^-)$ by J_z/v with an appropriate correlation, should yield two coupled PDEs for the bulk variables, the bulk density $c(z, t)$ and the net flux $J_z(z, t)$. Next a pseudo-equilibrium state for the flux is assumed in the PDE of $J_z(z, t)$ such that $\partial J_z/\partial t \simeq 0$. A constitutive relationship relating $J_z(z, t)$ to the bacterial bulk density $c(z, t)$ and the gradient $\partial c(z, t)/\partial z$, in form of the Fickian expression of Eq. (35b), is then derived. While the mass conservation equation for the bulk density $c(z, t)$ is always attainable, the PDE for the cellular flux $J_z(z, t)$ only exists if the flux J_z is nonzero, i.e. the angular density distribution is anisotropic. To overcome possible degeneracy for the flux PDE, a nonzero ξ is assumed first. Then we derive the equilibrium Fickian flux expression and pursue the limiting situation $\xi \to 0$ while holding θ_0 constant.

In view of the location of θ_0 and the integration limits in all subpopulation quantities defined in previous sections, Segel's approach again needs to be evaluated separately for the two situations, $\theta_0 \in [0, \pi/2]$ and $\theta_0 \in [\pi/2, \pi]$. However, some results for both situations are identical, such as the net z-flux,

$$J_z = v\frac{c}{2} n_s \xi (1 - u_0)^2 \left(\frac{2 + u_0}{6}\right) + O(\xi^2), \quad \theta_0 \in [0, \pi]. \tag{36}$$

If we consider only the leading terms, J_z is proportional to ξ, indicating that the flux only exists as a result of the spatial chemical gradient. The same conclusion holds for the difference of the subpopulation densities $(n^+ - n^-)$.

The quantity $v(n^+ - n^-)$, representing a similar measure of bacterial net migrations in the z-axis, has a correlation with the net flux J_z. As both quantities go to zero in the limit of $\xi \to 0$ while keeping θ_0 fixed, the ratio of J_z to $v(n^+ - n^-)$ remains a constant value, which is, however, different for the two ranges of θ_0. These flux ratios for both situations are listed in Tables 1 and 2 respectively, and will be used later in the substitution of $v(n^+ - n^-)$ for J_z.

Following our previous approach (Chen *et al.*, 1999) after some algebra and rearrangement, we obtain

$$\mu = \frac{v^2}{2}\left(\frac{2+u_0}{3}\right)\left[1 + n_s\xi(1-u_0)^2\left(\frac{1+2u_0}{12}\right)\right]\Big/ (\tilde{p}_t^- + \tilde{p}_t^+)p_r \tag{37a}$$

and

$$V_c = v\left(\frac{2+u_0}{3}\right)\frac{\tilde{p}_t^- - \tilde{p}_t^+}{\tilde{p}_t^- + \tilde{p}_t^+} \tag{37b}$$

for $\theta_0 \in [0, \pi/2]$, and

$$\mu = \frac{v^2}{2}\left[\frac{(1-u_0)^2(2+u_0)}{3(1-2u_0-u_0^2)}\right] \times \left\{1 + n_s\xi(1+u_0)^2\left(\frac{1-2u_0}{12}\right)\right\}\Big/ (\tilde{p}_t^- + \tilde{p}_t^+)p_r \tag{38a}$$

and

$$V_c = v\left[\frac{(1-u_0)^2(2+u_0)}{3(1-2u_0-u_0^2)}\right]\frac{\tilde{p}_t^- - \tilde{p}_t^+}{\tilde{p}_t^- + \tilde{p}_t^+} \tag{38b}$$

for $\theta_0 \in [\pi/2, \pi]$.

Table 1
Summary of the asymptotic expansion results for $\theta_0 \in [0,\pi/2]$

	$\theta_0 \in \left[0, \frac{\pi}{2}\right]$	
$\frac{J_z}{v(n^+ - n^-)}$	$\frac{2+u_0}{3}$	
$\mu \Big/ \left(\frac{v^2}{2p_0}\right)$	$\left(\frac{2+u_0}{3}\right)\left[1 + \frac{\xi}{6}(1-u_0)^2(2+u_0)\right] + O(\xi^2)$	
	$= \mu_0[1 + \mu_1\xi] + O(\xi^2)$	(39a)
$\frac{V_c}{v\xi/3}$	$\frac{(1-u_0)^2(2+u_0)}{4} + O(\xi)$	
	$= V_{c,0} + O(\xi)$	(39b)

Table 2
Summary of the asymptotic expansion results for $\theta_0 \in [\pi/2,\pi]$

	$\theta_0 \in \left[\frac{\pi}{2}, \pi\right]$	
$\frac{J_z}{v(n^+ - n^-)}$	$\frac{1}{3}\frac{(1-u_0)^2(2+u_0)}{(1-2u_0-u_0^2)}$	
$\mu \Big/ \left(\frac{v^2}{2p_0}\right)$	$\frac{(1-u_0)^2(2+u_0)}{3(1-2u_0-u_0^2)}\left[1 + \frac{\xi}{6}(2-3u_0-u_0^3)\right] + O(\xi^2)$	
	$= \mu_0[1 + \mu_1\xi] + O(\xi^2)$	(40a)
$\frac{V_c}{v\xi/3}$	$\frac{(1-u_0)^2(2+u_0)}{4} + O(\xi)$	
	$= V_{c,0} + O(\xi)$	(40b)

Eqs. (37a), (37b) and (38a), (38b), together with Eqs. (34a) and (34b) for the exponential mean tumbling frequencies are the appropriate expressions to employ when the chemical gradients Γ or ξ are larger than unity. The use of the exponential mean tumbling frequencies avoids extrapolating $\tilde{p}t^{\pm}$ to negative values when the perturbation theory does not apply (Γ and ξ greater than one). Although our results were derived based on the expanded tumbling frequencies with respect to small chemical gradients, numerically we found that applying the exponential mean tumbling frequencies to situations of large chemical gradients still yields good agreement to the numerical solutions obtained from the complete cell balance Eq. (2). Nevertheless, we continue to pursue the explicit expansion expressions for μ and V_c in the context of small chemical gradients by substituting in the expanded mean tumbling frequencies.

5.1.1. Asymptotic expansion

As noted in the previous section, our analysis was based on a simple turning probability density function $W(\alpha) = 1/2$, which results in a one-dimensional reversal probability $p_r = 1/2$. Using $p_r = 1/2$ and the equilibrium expansion coefficient $n_s = 1$, we explicitly expressed the random motility coefficient μ and chemotactic velocity V_c in terms of bacterial intrinsic properties by linearly expanding the mean tumbling frequencies and then collecting the first two leading terms [$O(1)$ and $O(\xi)$]. The resulting random motility coefficient was nondimensionalized (see Tables 1 and 2) with the following zeroth- and first-order dimensionless coefficients:

$$\mu_0 = \frac{2+u_0}{3} \quad \text{and} \quad \mu_1 = \frac{1}{6}(1-u_0)^2(2+u_0)$$

for $\theta_0 \in [0, \pi/2]$, and

$$\mu_0 = \frac{(1-u_0)^2(2+u_0)}{3(1-2u_0-u_0^2)} \quad \text{and} \quad \mu_1 = \frac{1}{6}(2-3u_0-u_0^3)$$

for $\theta_0 \in [\pi/2, \pi]$.

The nondimensionalization was made such that the leading term μ_0 happens to be the ratio of J_z to $v(n^+ - n^-)$. Intuitively, the unperturbed term μ_0 should be independent of any parameters associated with anisotropic chemical gradients, as this is true for the smooth-type p_t (Chen *et al.*, 1999). The false θ_0-dependency in μ_0 apparently arises from adopting the one-dimensional approach. The dimensionless chemotactic velocity was also presented in Tables 1 and 2 where

$$V_{c,0} = \tfrac{1}{4}(1 - u_0)^2(2 + u_0)$$

for $\theta_0 \in [0, \pi]$. The chemotactic velocity is nondimensionalized with respect to the maximum chemotactic velocity $v\xi/3$, i.e. the value at $\theta_0 = \pi$. Note that ξ and Γ by their definitions have no units.

Several points need to be emphasized. First, we note that the leading order of the *dimensional* random motility coefficients given by Eqs. (39a) and (40a) is $O(1)$, whereas the leading order of the *dimensional* chemotactic velocity in Eqs. (39b) or (40b) is only $O(\xi)$. This is because by nature chemotactic velocity only exists when ξ is nonzero. Unlike μ, the magnitude of V_c is therefore associated with ξ. Under extremely small chemical gradients the chemotactic velocity is effectively proportional to ξ. However, the proportionality is valid only based on the *first-order* perturbation theory. Hence the result for the dimensionless chemotactic velocity, $V_{c,0}$, is accurate to the first order of ξ and monotonically increases from zero at $\theta_0 = 0$ to one at $\theta_0 = \pi$. A larger angle θ_0 means a larger fraction of $c(z, t)$ can respond to a chemical gradient through the regulation of the tumbling frequency, thus resulting in a stronger chemotactic migration. Notice that the change in the angle θ_0 can be achieved without increasing the magnitude of ξ but by only varying the value for Γ. Second, the dimensionless random motility coefficient of the zeroth order μ_0 in Segel's one-dimensional approach is defined to be the ratio of the cellular flux J_z to $v(n^+ - n^-)$. Accordingly, the ratio of J_z to $v(n^+ - n^-)$ increases to one as $\theta_0 \to 0$. At $\theta_0 = 0$ the bacterial tumbling frequency does not respond to any chemical gradients, and the dimensionless coefficient μ_0 therefore should yield a value of 2/3 (Chen, 1997) instead of 1. This peculiar discontinuous behavior of μ_0 at $\theta_0 = 0$ ($u_0 = 1$), i.e., $\Gamma + \xi = 0$, can be explained by the two limiting cases that approach the zero gradient point $\Gamma + \xi = 0$ from opposite sides,

$$\lim_{\Gamma + \xi \to 0+} \mu_0 = 1, \qquad \lim_{\Gamma + \xi \to 0-} \mu_0 = \tfrac{2}{3}.$$

Because of this *one-dimensional* definition, a discontinuity exists as $\theta_0 \to 0$.

5.1.2. One-dimensional RTBL model

To facilitate understand the underlying reason behind the discontinuity and why the flux ratio rises up to one, we next examine a *true* one-dimensional model (the so-called RTBL model, Rivero *et al.*, 1989) in which bacterial motion is restricted to the direction of a one-dimensional chemical gradient. The analytical results in Tables 1 and 2 will be qualitatively compared with those proposed by the one-dimensional model of Rivero *et al.* (1989). We expect results from both models to be different because of the different constraints in dimensionality. However, due to the axial symmetry and the same one-dimensional approach, it is anticipated that both models will yield similar behaviors under certain circumstances. More importantly, the existence of the discontinuity at $\theta_0 = 0$ discussed before may be better understood from studying the one-dimensional model of Rivero *et al.* (1989).

Assuming that bacteria swim one-dimensionally along the z-axis with a one-dimensional speed s and a reversal probability $p_r = 1/2$, the corresponding expressions of the random motility coefficient and chemotactic velocity, based on the same non-smooth tumbling frequency, are

$$\mu^{\mathrm{RTBL}} = \frac{2s^2}{p_0}\{1 + \exp[-(\Gamma + \xi)]\}^{-1} \tag{41a}$$

and

$$V_c^{\mathrm{RTBL}} = s\frac{1 - \exp[-(\Gamma + \xi)]}{1 + \exp[-(\Gamma + \xi)]}, \tag{41b}$$

both of which are adopted from Eqs. (29) and (30) of the paper of Rivero *et al.* (1989), except that $v(\mathrm{d}N_b/\mathrm{d}a)(\partial a/\partial t)$ is replaced by Γ, and $vs(\mathrm{d}N_b/\mathrm{d}a)(\partial a/\partial z)$ is replaced by ξ.

In the one-dimensional RTBL model it is meaningless to discuss an angle range since bacterial swimming direction only allows two choices: either $\theta = 0$ or $\theta = \pi$. Nevertheless, we still defined $\cos\theta_0 = -\Gamma/\xi$ and regarded $\cos\theta_0$ as a proportionality factor between Γ and ξ. Substituting in the relation $\Gamma = -\xi\cos\theta_0$ and expanding the exponential functions, we rewrote Eqs. (41a) and (41b), in the small gradient limit, as

$$\mu^{\mathrm{RTBL}} \Big/ \left(\frac{s^2}{p_0}\right) = 1 \cdot \left[1 + \frac{\xi}{2}(1 - u_0)\right] + O(\xi^2)$$
$$= \mu_0^{\mathrm{RTBL}}[1 + \mu_1^{\mathrm{RTBL}}\xi] + O(\xi^2) \tag{42a}$$

where

$$\mu_0^{\mathrm{RTBL}} = 1, \quad \mu_1^{\mathrm{RTBL}} = \tfrac{1}{2}(1 - u_0)$$

and

$$V_c^{\mathrm{RTBL}}/(s\xi) = \frac{(1 - u_0)}{2} + O(\xi) = V_{c,0}^{\mathrm{RTBL}} + O(\xi) \tag{42b}$$

in which

$$V_{c,0}^{\mathrm{RTBL}} = \tfrac{1}{2}(1 - u_0).$$

Again, u_0 indicates $\cos\theta_0$ in above expressions. The nondimensionalization also was arranged in such a way that

the leading term μ_0^{RTBL} is the ratio of J_z^{RTBL} to $s(n^+ - n^-)$ and that $V_{c,0}^{\mathrm{RTBL}}$ ranges between zero and unity. One sees that Eq. (42a) gives a constant μ_0^{RTBL} $(=1)$ due to the one-dimensional constraint, while Eqs. (39a) and (40a), derived from a three-dimensional model but processed by a one-dimensional approach, have a θ_0-dependent μ_0 ranging between 2/3 and 1. The difference clearly results from the intrinsic dimensionality that defines bacterial motion in space. Accordingly, we also see a transition as Eq. (39a) gradually exhibits characteristics of an intrinsic one-dimensional model. When θ_0 is close to zero, the bacterial angular density distribution on the angular spherical surface is almost isotropic except within the small cone confined within the range $[0, \theta_0]$. Thus bacteria swimming at an angle θ between $[\theta_0, \pi - \theta_0]$ have zero contribution to either the flux J_z or the density difference $(n^+ - n^-)$ due to an exact cancellation from their complementary density at $\pi - \theta$. Only those swimming within the small angle range $(0, \theta_0)$ have an unbalanced density concentration relative to those in their corresponding complementary angles. For a sufficiently small θ_0, the bacteria swimming inside $[0, \theta_0]$ and $[\pi - \theta_0, \pi]$ swim essentially parallel to the z-axis. Due to this one-dimensional definition for μ_0, at small θ_0 the motion of the bacteria dominating the macroscopic transport behaviors becomes effectively one-dimensional. This explains why the dimensionless random motility μ_0, as $\theta_0 \to 0$, approaches unity as predicted by Eq. (42a) which assumes one-dimensional cell motion.

Other than that, both models exhibit similar trends for parameters μ_1 and $V_{c,0}$. For instance, $V_{c,0}$ and $V_{c,0}^{\mathrm{RTBL}}$ both begin at zero $(\theta_0 = 0)$ and monotonically increase to one at $\theta_0 = \pi$. The same is true for μ_1 and μ_1^{RTBL}. Fig. 5 depicts all the dimensionless coefficients μ_0, μ_1, and $V_{c,0}$ versus θ_0 from both models. Except for μ_0, the one-dimensional RTBL model gives similar predictions for the dimensionless coefficients μ_1 and $V_{c,0}$. However, the functional dependence on $\cos\theta_0$ is different, a consequence of the different restrictions on the intrinsic dimension.

5.2. Three-dimensional angular integration

The one-dimensional approach results in a discontinuity at θ_0, and therefore is incorrect. This error results from the inappropriate employment of Segel's one-dimensional methodology to treat a three-dimensional transport equation. Note that when the anisotropic tumbling is smooth in the whole velocity space, such a discontinuity does not appear. Since the bacterial angular density is available, following Schnitzer's (1993) approach, we directly integrated Eq. (2) by the first-order

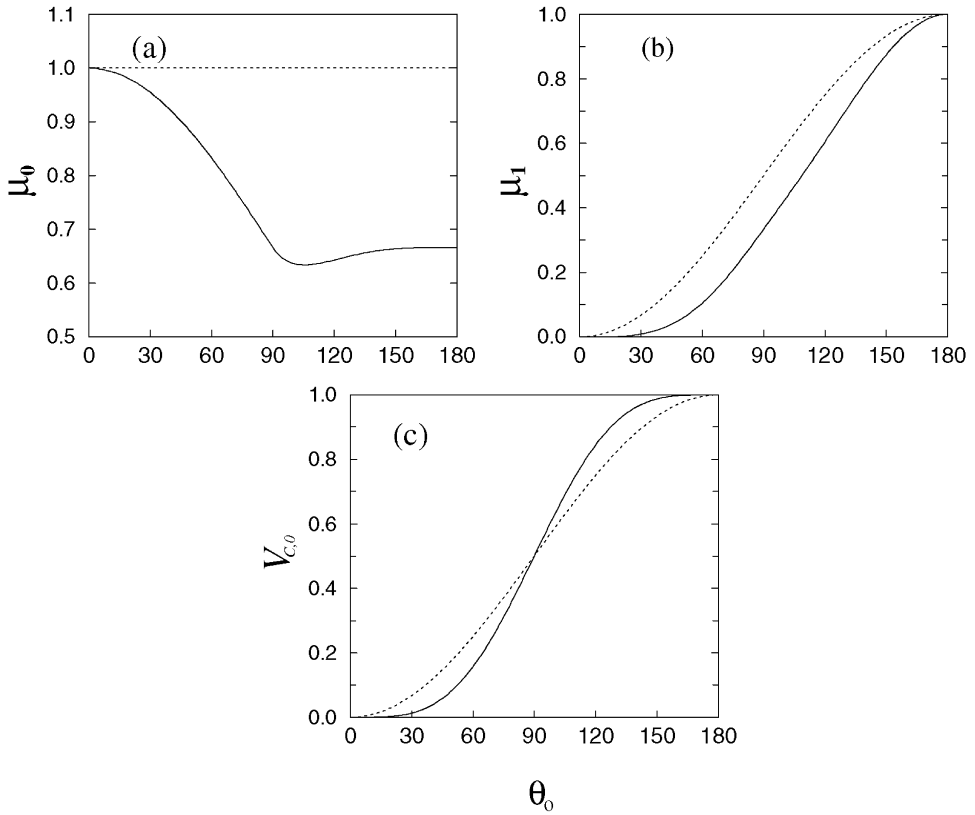

Fig. 5. Comparisons of dimensionless transport coefficients for (a) μ_0, (b) μ_1, and (c) $V_{c,o}$ from the results of perturbation theory (solid lines) and the one-dimensional RTBL model (dashed lines).

angular moment over the spherical velocity space and obtained

$$\mu \Big/ \left(\frac{v^2}{2p_0}\right) = \frac{2}{3}\left[1 + \frac{\xi}{8}(1-u_0)(1-3u_0+u_0^2+u_0^3)\right] + O(\xi^2) \tag{43a}$$

and

$$\frac{V_c}{v\xi/3} = \frac{(1-u_0)^2(2+u_0)}{4} + O(\xi). \tag{43b}$$

The integration is straightforward and thus will not be addressed here. Readers are referred to Schnitzer (1993) or Chen (1997) for details. Eq. (43a) predicts a constant and continuous $\mu_0 = 2/3$ in its unperturbed (zeroth-order) term and is consistent both at $u_0 = \pm 1$ with respect to the theoretical results of Chen *et al.* (1999). In the next numerical section, we showed that Eq. (43a) is the correct expression for the random motility coefficient. Surprisingly, the chemotactic velocity is unaffected by the adopted approach: Eq. (43b) is the same as Eqs. (39b) and (40b). We also found an interesting agreement between our theoretical V_c and that of Lovely and Dahlquist (1975), who derived the equilibrium chemotactic velocity in terms of integrals of bacterial mean run time distributions over three-dimensional velocity space,

$$V_c = v\frac{\int_{-1}^{1} T(z,\theta;\xi)\cos\theta\,\mathrm{d}(\cos\theta)}{\int_{-1}^{1} T(z,\theta;\xi)\,\mathrm{d}(\cos\theta)}. \tag{44}$$

Here $T(z,\theta;\xi)$ denotes the mean run time distribution in θ direction, and is equal to $1/p_t(z,\theta;\xi)$ for a valid Poisson process. For a small ξ, we similarly expanded $T(z,\theta;\xi)$ in a Taylor series and then took the linear expression by truncating the higher-order terms. It can be easily verified that substituting this linear form for T into Eq. (44) and integrating yields the same leading term as Eq. (43b).

6. Finite element solutions

To further validate our perturbation analysis in the prediction of the random motility coefficient and chemotactic velocity, we numerically solved the axisymmetrical Alt equation (2) using the original biphasic exponential tumbling frequency, Eq. (9). The algorithm used was Galerkin finite element method (FEM) adopting rectangular grids in the two dimensional domain constructed by the z and θ axes. Also employed were quadrilateral interpolation functions as developed by Frymier *et al.* (1994) to linearly interpolate values between nodal densities. However, a nonuniform grid discretization was adopted to take advantage of our *a priori* knowledge about the density distribution in θ: the area near θ_0 has more dense grids in the θ direction. Therefore, a significantly fewer number of elements was required to achieve the accuracy comparable to numerical solutions using a uniform discretization. Because there were no unusual characteristics about the assembly of the global conductance matrices in Galerkin FEM, we skipped the details here except that the solution to Eq. (2) could be represented by the following system of linear algebraic equations in matrix form:

$$\mathbf{P}\frac{\partial \mathbf{n}}{\partial t} = \mathbf{U}\mathbf{n} - \mathbf{T}\mathbf{n} + \mathbf{g} + \mathbf{b}$$

where $\mathbf{n}$ is the column vector representing the nodal values of cell density, the square coefficient matrices $\mathbf{P}$ and $\mathbf{U}$ correspond to the time-derivative term and the convective term, respectively. Both $\mathbf{P}$ and $\mathbf{U}$ are constant coefficient matrices and only need to be constructed once. $\mathbf{T}$ represents the tumbling term divergent from the angle θ. The integral term involved with the coupled tumbles and turns in all directions in Eq. (2) was taken to be explicit and was represented by the column vector $\mathbf{g}$. The vector $\mathbf{b}$ represents the boundary conditions. Gaussian quadrature was used in the numerical integration in $\mathbf{g}$. For the transient case of a nonuniform attractant distribution, $\mathbf{T}$ and $\mathbf{g}$ will be updated at each time step according to the biphasic tumbling frequency and the spatial and temporal attractant gradients.

In this study, the z–θ domain was generally discretized into 800 elements (40×20) with 861 nodes. Further details regarding the numerical scheme can be found in Frymier *et al.* (1994). To meet the assumptions made in the analysis, we restricted our numerical solution to the case of $W(\alpha) = 1/2$ only. Three examples were presented. The first two enable us to calculate the chemotactic velocity and random motility coefficient independently, in which Γ and ξ do not change over time and space. Since the derivations of the random motility coefficient and chemotactic velocity require the equilibrium assumption, we were only interested in the steady-state solutions. The third example was somewhat more complex in that Γ and ξ become functions of time and space with magnitudes larger than one.

Example 1. To calculate the chemotactic velocity, we assumed a uniform bacterial suspension in a capillary tube as the initial condition, $n(z,t_0,\theta) = c_0/2$. At $t = t_0$, a constant spatial attractant gradient ξ and temporal attractant Γ along the z-axis were suddenly imposed over the computational domain. Bacteria within the domain sensing the spatial gradient ξ started migrating up this spatial gradient in the positive z direction and moved out of the domain at the right boundary $z = L$. A schematic view of the computational domain, showing the dimensions and the boundary conditions, is provided in Fig. 6a. We further assumed that the flow rate of chemotactic bacteria out of the spatial domain at one end ($z = L$) was exactly the same as the rate flowing in at the

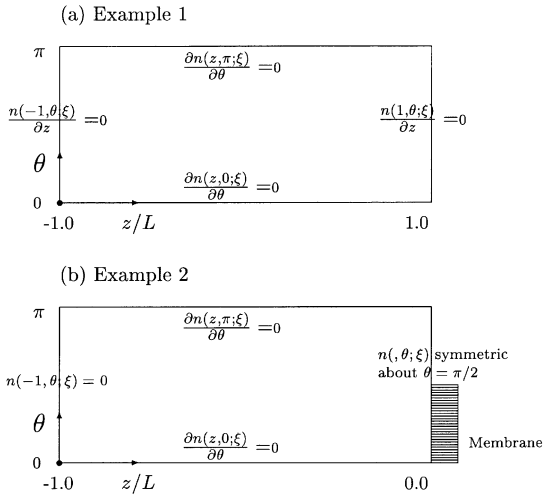

Fig. 6. Schematic diagrams for the computational domain and the boundary conditions in the numerical experiments.

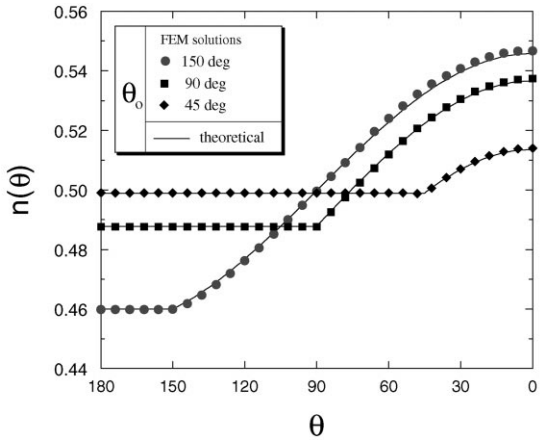

Fig. 8. Comparisons of the bacterial density distribution functions $n(\theta)$ between numerical solutions and theoretical predictions, Eq. (21), for $\xi = 0.1$.

other end ($z = -L$), so that no local variation of bacterial density existed along z, i.e. $\partial n(z, \theta, t)/\partial z = 0$. The steady-state cellular flux J_z was calculated from integrating $n(z, \theta; \xi)$ over θ according to Eq. (6b). The chemotactic velocity was determined from the local flux J_z and the local concentration c since the gradient in bacterial concentration $\partial c/\partial z$ was zero.

Fig. 7 displays one of our numerical results for $\xi = 0.3$ and $\theta_0 = 90^\circ$ (indicating $\Gamma = 0$). The zero-gradient boundary condition was used on all boundaries although physically bacteria were entering the domain at the left ($z/L = -1$) and leaving at the right ($z/L = +1$). Chemotactic flow was therefore from left to right. The computational iteration was repeated until steady state was achieved, as defined by the criterion $\mathrm{MAX}(|n(z, \theta, t + \Delta t; \xi) - n(z, \theta, t; \xi)|/c_0) \leqslant 10^{-4}$. The calculated steady-state density distribution does not vary along the z-axis. However, the distribution along θ deforms from the initially uniform distribution. As expected, the density distribution in the range $[\theta_0, \pi]$ is still uniform but becomes slightly lower than the initial value, which results from the compensation made by the elevated $n(z, \theta, t)$ in $[0, \theta_0]$. The relative scale is shown in Fig. 8, where the dimensionless density distributions along θ obtained separately from the FEM solutions and our theoretical perturbation result were compared for three different values of θ_0. The equilibrium values for $n_0 (= \mathscr{K})$ and $n_s (= 1)$ were used in calculating the theoretical lines. The theoretical lines agree well with the finite element solutions, especially for small values of θ_0.

Since the numerical solution for the number density distribution along θ is available now, we can evaluate the flux and the local bulk density to obtain the chemotactic velocity. The numerically evaluated chemotactic velocities at different values of θ_0 are compared with theoretical solutions given by Eq. (43b) in Fig. 9. Very good agreement between numerical solutions (solid circles) and theoretical prediction (solid line) is observed. We also note that at $\theta_0 = 180^0$, V_c recovers

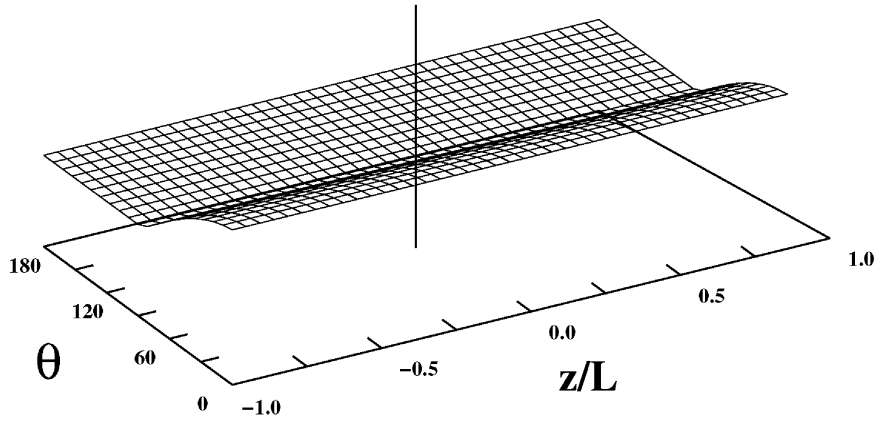

Fig. 7. Two-dimensional numerical solution of the simplified Alt's cell balance equations applied to Example 1 for $W(\alpha) = 1/2$ at $\xi = 0.3$ and $\theta_0 = 90^\circ$.

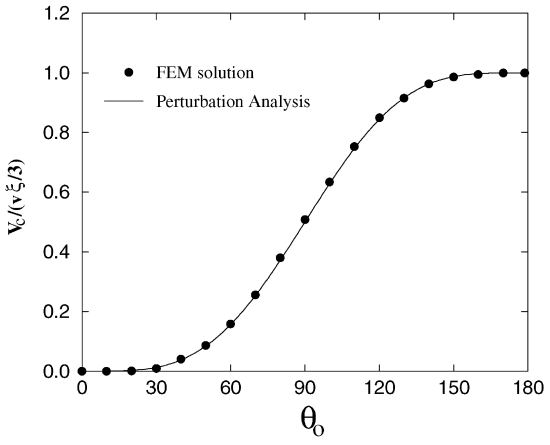

Fig. 9. Plot of the dimensionless chemotactic velocities versus θ_0 at $\xi = 0.1$.

back the expression $v\xi/3$ as previously derived (Chen *et al.*, 1999).

Example 2. To calculate the random motility coefficient, one cannot allow $\partial c/\partial z = 0$. To design such a nonuniform situation, we assumed that bacteria in a capillary tube were still responding to constant Γ and ξ. However, one end of the tube ($z = 0$) was sealed with a membrane permeable only to attractant molecules. The constant spatial attractant gradient can be established by providing a fixed attractant concentration at the outside margin of the membrane as shown in Fig. 6b. The bacterial population near the sealed end then migrated toward the attractant source and built up a spatially sharp density profile near $z = 0$ due to the impermeable boundary condition, while the random motility (analogous to molecular diffusivity) counteracted the chemotactic flow and tended to diffuse the profile. Therefore, a steady-state profile of the bacterial bulk density along z-axis can be established. At steady state, the net bacterial flux was zero everywhere, leaving the cellular diffusion term balanced by the chemotactic term. Thus the random motility coefficient was estimated from the local bacterial density $c(z;\xi)$ and the gradient $\mathrm{d}c(z;\xi)/\mathrm{d}z$. The chemotactic velocity V_c was estimated from Eq. (43b). Then μ was calculated as $V_c\, c\,(\mathrm{d}c/\mathrm{d}z)^{-1}$.

The numerical solution within the z–θ domain for this example is shown in Fig. 10. The boundary condition at the dimensionless position $z/L = -1$ is $n(-1, \theta; \xi) = 0$. At $z/L = 0$ where the membrane was sealed, we assumed a reflective boundary condition. That is, a symmetric $n(0, \theta; \xi)$ about $\theta = \pi/2$ was used to ensure zero net flux. Note that the equilibrium profile in Fig. 10 also exhibits symmetry about the central line $\theta = \pi/2$ throughout the domain, demonstrating how the boundary conditions can affect the whole profile. The symmetry is not a surprising result since at steady state the solution must support the zero-flux condition everywhere. One may look at Eq. (6b) that defines the net flux in the z-axis. Since the integrand '$\sin\theta\cos\theta$' is an odd function about $\theta = \pi/2$ in $[0, \pi]$, the symmetrical density profile $n(0, \theta; \xi)$ about $\theta = \pi/2$ is sufficient, but not necessary, to ensure the zero flux for the integration.

Next the dimensionless random motility coefficient was numerically evaluated along the z-axis. A typical result for the random motility coefficient at a specific θ_0 is shown in Fig. 11. A fairly constant value for the random motility coefficient throughout the whole domain is exhibited for a given pair of constant ξ and θ_0 values. The fluctuation of data at the left end is because both the density concentration c and the gradient $\mathrm{d}c/\mathrm{d}z$ are extremely small there (also see the $z - \theta$ density profile in Fig. 10), which consequently results in large truncation errors. Fig. 12 shows the dimensionless random motility coefficient versus θ_0, together with theoretical

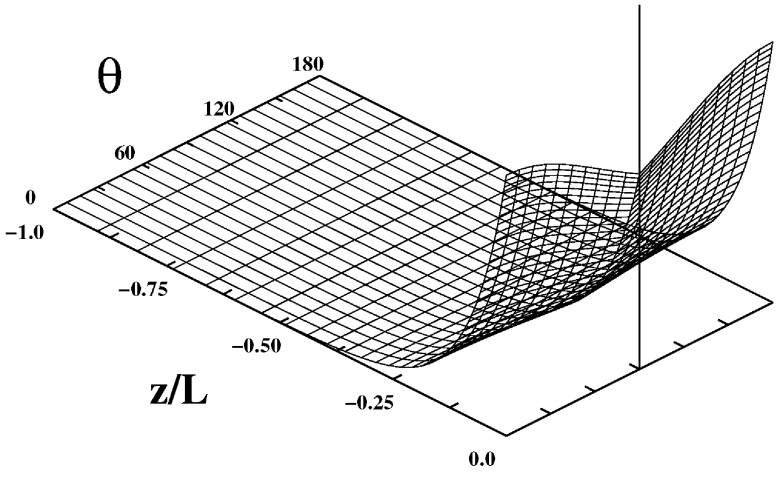

Fig. 10. Two-dimensional numerical solution of the simplified Alt's cell balance equations applied to Example 2 at $\xi = 0.3$ and $\theta_0 = 90°$.

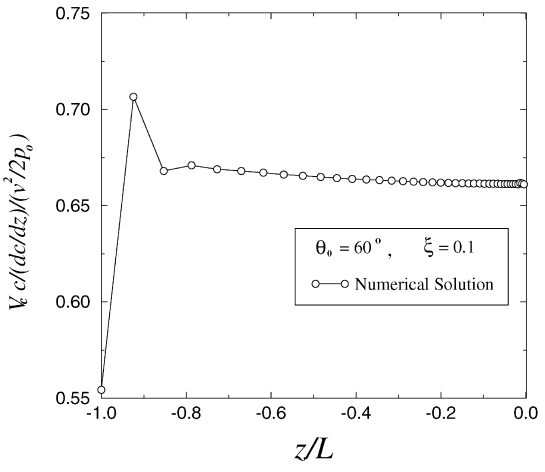

Fig. 11. An example of the numerical results of the dimensionless random motility coefficients along the z-axis.

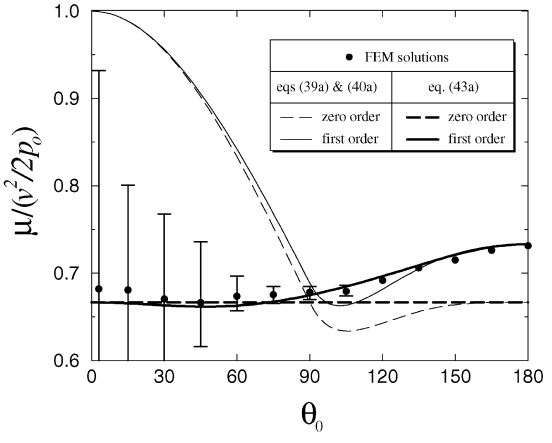

Fig. 12. Plot of the dimensionless random motility coefficient versus θ_0 at $\xi = 0.1$.

predictions. The bold and the thin dashed lines are the zero-order solutions of Eq. (43a) and Eqs. (39a) and (40a), respectively. They are provided here as base lines for comparing the deviations between the unperturbed and perturbed solutions. Note that the value of the dimensionless random motility at $\theta_0 = 0$ cannot be numerically attained with precision since both V_c and $\mathrm{d}c/\mathrm{d}z$ are zero at $\theta_0 = 0$. Consequently, numerical fluctuations increase as θ_0 approaches zero. Although considerable uncertainty (which depends on the initial guess of the bacterial density profile) arises in this example, we find that much of the numerical data (solid circles) is closer to the predictions of the three-dimensional angular integration at the region where θ_0 is less than $\pi/2$, indicating that Eq. (43a) is the correct expression. As θ_0 approaches π, the numerical solution approaches $2(1 + \xi)/3$, consistent with our previous theoretical analysis (Chen *et al.*, 1999) adopting the smooth linear expansion $p_t \simeq p_0(1 - \xi\cos\theta)$.

Example 3. The generality of both examples given above is limited by the assumption of constant ξ and Γ. As expected, the numerical results are in good agreement with our perturbation analysis. In actuality, however, the chemical gradients may vary with time and location to different extents and may not be small. Thus, the question naturally arises to the validity of the constant-gradient approximation which ultimately led to our theoretical predictions. Because of this, we intend to relax this restriction in the next example which will allow us to examine the usefulness of our theory.

A good example to test our theory is the setup of the stopped flow diffusion chamber (SFDC) developed by Ford and Lauffenburger (1991) in which an initially uniform bacterial density population responded to a step change in attractant concentration. The reason for choosing the SFDC assay is because it provides well-characterized chemical gradients that vary with time and space. The experimental conditions were such that during flow, two uniform bacterial suspensions differing only in attractant concentration were contacted by impinging flow in the center of a rectangular chamber and a step change in attractant concentration was maintained. Once the flow had been stopped, the attractant in one-half of the chamber ($0 \leqslant z/L \leqslant 1$) started to diffuse into the other half ($-1 \leqslant z/L \leqslant 0$), creating transient temporal and spatial attractant gradients in the z-axis. As bacteria sensed and responded to the gradients, a high-density band of bacteria formed immediately and migrated toward higher attractant concentrations as time progressed and as the attractant gradient decayed. The concentration of the attractant, $a(z, t)$, is described by

$$a(z, t) = a_0\left[1 + \mathrm{erf}\left(\frac{z}{\sqrt{4D_a(t + t_s)}}\right)\right], \tag{45}$$

and the spatial and temporal gradients of $a(z, t)$ are

$$\frac{\partial a(z, t)}{\partial z} = \frac{a_0}{\sqrt{\pi D_a(t + t_s)}}\exp\left(-\frac{z^2}{4D_a(t + t_s)}\right) \tag{46}$$

and

$$\frac{\partial a(z, t)}{\partial t} = -\frac{z}{2(t + t_s)}\frac{\partial a(z, t)}{\partial z} \tag{47}$$

where a_0 is the height of the step attractant concentration, D_a the diffusivity coefficient of attractants, t_s an experimental off-set time used to avoid the singularity at zero time. Then Γ and ξ at any location and time are determined accordingly. It is emphasized that the purpose of performing those numerical experiments is to validate our theoretical conclusions, but not to compare simulation results with actual experiments. Therefore, we did not specifically consider the saturation effect of the receptors here since it does not affect the comparison between the numerical solutions and theoretical predictions, and hence is not our concern in this paper. We set

Table 3
Parameter values used in finite element solutions

Parameter	Symbol	Value	Units
z-domain length scale	L	0.4	cm
Bacterial 3-D swimming speed	v	22	μm/s
Initial attractant concentration	a_0	1.0	mM
Attractant diffusivity coefficient	D_a	5×10^{-6}	cm^2/s
Derivative of bound receptors	dN_b/da	1.0	receptors/mM
Scaling factor in tumbling responses	ν	15.0	s/receptor
Basal tumbling frequency	p_0	0.3	1/s
SFDC off-set time	t_s	5.0	s

$dN_b/da = 1$ and adjusted the value of v by assuming the factor dN_b/da to be absorbed into v. Upon analyzing experimental measurements of the chemotactic sensitivity of *E. coli* in Ford and Lauffenburger (1991), we decided $v = 15$[2] was an adequate value in our simulation. All the parameters used in this simulation were summarized in Table 3.

We found that employing values of those parameters in Table 3 produced a spatial attractant gradient ξ as high as 8.5 at the beginning of our simulation, which strongly violates the small gradient assumption. Note that the off-set time assumed here was $t_s = 5$ s, while in the paper of Ford and Lauffenburger (1991) $t_s = 10$ s was used. Thus, the setting of our parameter values is severe enough to make our final conclusion general.

Since in this example all three quantities J_z, c, and $\partial c/\partial z$ vary over time and location and do not necessarily equal zero, one cannot independently determine both parameters μ and V_c from a single relation as we did in the previous two examples. However, one still can numerically evaluate the ratio of J_z to $v(n^+ - n^-)$. Fig. 13 displays such results in which the solid lines were produced from perturbation theory, namely, the μ_0 in Tables 1 and 2. Some data close to both boundaries $z/L = \pm 1$ had been screened out at small times ($t = 1, 10$ min) because both J_z and $v(n^+ - n^-)$ there were still undeveloped. We found the agreement of the numerical results with our theory satisfactory even though some deviations occurred at short times. Furthermore, both theoretical lines and numerical results converge together as time proceeds. Note that for this system $\partial a/\partial z$ is always positive

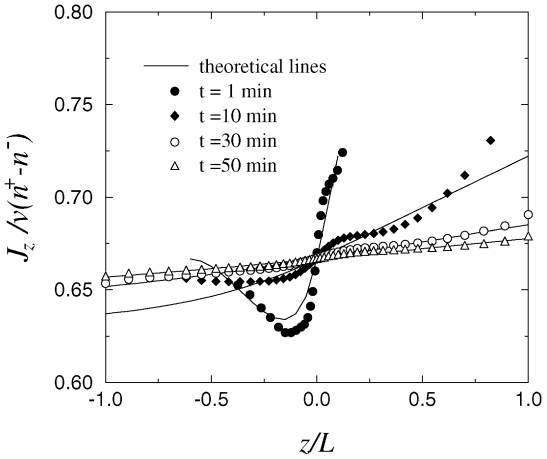

Fig. 13. Comparisons of the flux ratios of J_z to $v(n^+ - n^-)$ between theory and numerical solutions in Example 3.

between $-1 \leqslant z/L \leqslant 1$. For $z/L > 0$, $\partial a/\partial t$ is negative and for $z/L < 0$, $\partial a/\partial t$ is positive. Therefore, in the region $z/L \in [0, 1]$, one can conclude that $\theta_0 \in [0, \pi/2]$, while in the region $z/L \in [-1, 0]$, $\theta_0 \in [\pi/2, \pi]$. According to the trends shown in Fig. 12, we anticipated that the numerical ratios in Fig. 13 will go up above 2/3 in the region $z/L \geqslant 0$, and fall slightly below 2/3 in the region $z/L \leqslant 0$. The agreement exhibited in Fig. 13 is also reflected in the comparisons of the bacterial bulk concentration profiles in the SFDC as shown in Fig. 14. The angular density $n(z, \theta, t; \xi)$ of Eq. (2) was numerically solved by FEM, and then integrated to yield spatial profiles of $c(z, t; \xi)$ over times (dashed lines). They were compared with the analytical ones (solid lines) obtained from solving the set of two one-dimensional PDEs, Eqs. (35a) and (35b), in terms of c and J_z. The transport parameters μ and V_c were estimated by Eqs. (37a), (37b) and (38a), (38b), together with the use of the exponential mean tumbling frequencies in Eqs. (34a) and (34b). However, the dimensionless leading term $(2 + u_0)/3$ in Eq. (37a) was modified to be a constant 2/3 to avoid the discontinuity. Although this employment is purely empirical and not theoretically based, we note that it does have

[2] In the paper of Ford and Lauffenburger (1991), $V_c = \chi_o \nabla_z a/K_d(1 + a/K_d)^2$, where $\chi_o = \nu s^2 R_t$ with R_t being the total receptors per cell. Since they used the relationship $s = v/\sqrt{3}$, their expression for V_c is the same as Eq. (43b). Experimentally they found $\chi_o = (8 \pm 3)\times10^{-5}$ cm^2/s. Assuming $\chi_o = 10\times10^{-5}$ and $a = K_d = 0.08$ mM (Ford and Lauffenburger, 1991), we equate $v^2\nu/3 = 10\times10^{-5}/4$, resulting in $\nu = 7.5\times10^{-5}/v^2$. If $v = 3\times10^{-3}$ cm^2/s, $\nu \simeq 8$. If $v = 2.2\times10^{-3}$ cm^2/s, $\nu \simeq 15$. We used the severe restriction $\nu = 15$ here to test our perturbation results.

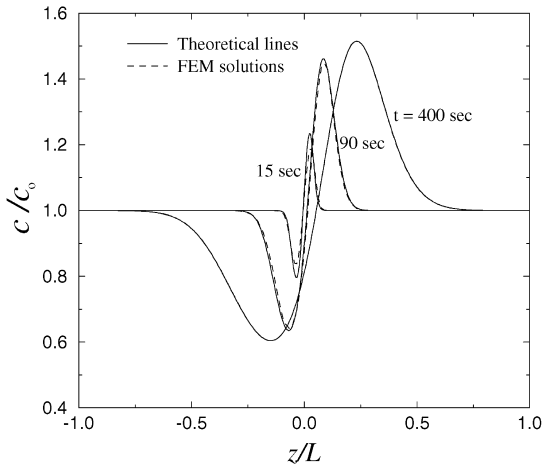

Fig. 14. Dimensionless bacterial bulk density profiles along the z-axis in the SFDC assay of Example 3.

some advantages. When both ξ and Γ are smaller than one, employing the above equations is virtually equivalent to adopting the asymptotic expansions, Eqs. (43a) and (43b), since under this situation the leading terms dominate anyway. On the contrary, when ξ and Γ are larger than one, adopting such empirical expressions is found to be no worse than the first-order perturbation results.

Both solutions in Fig. 14 exhibit small differences at small times. As time progresses, the magnitudes of attractant gradients Γ and ξ decay and both solutions gradually relax to identical ones. Although ξ is larger than one at the beginning of simulations, our modified solutions still give close predictions compared to the numerical solutions, which is also evidenced by the comparison of flux ratios in Fig. 13. The reason is attributed to the employment of the exponential mean tumbling frequencies such that the derived theory is not severely limited by the restriction $\xi \leqslant 1$. Calculations with μ and V_c corresponding to the asymptotic expansion, Eqs. (43a) and (43b), were also made but not presented here since they did not give a better fit to any of the numerical profiles in Fig. 14: The deviations from the numerical solutions at small times do not diminish as time progresses.

Apparently, the ultimate convergence of both solutions in Fig. 14 is partly due to the transiently decaying behaviors of attractant gradients designed in the example. Nevertheless, our results still showed that using the exponential mean tumbling frequencies gives more flexibility and extension in the application of our theoretical results to varying chemical gradients with arbitrary magnitudes, as long as the chemical gradients subside.

7. Conclusions

In this paper we applied a first-order perturbation analysis to the three-dimensional Alt's equation with a non-smooth biphasic tumbling frequency. Despite the use of the non-smooth function for the tumbling frequency, Alt's three-dimensional cell balance equation was reduced and approximately simplified into the same forms as Segel's one-dimensional phenomenological equations for the system possessing single axial symmetry. Two bacterial transport parameters: the random motility coefficient and the chemotactic velocity, were explicitly derived based on two conceptually distinct approaches. The dimensionless random motility μ_0, when derived from a one-dimensional approach, was defined as the ratio of bacterial flux J_z to the density difference $v(n^+ - n^-)$, and was found to exhibit a discontinuity as θ_0 approaches zero. The existence of this discontinuity was attributed to the incorporation of the one-dimensional approach and the non-smooth tumbling frequency characterized by θ_0. The expression for the chemotactic velocity was unaffected and agreed with that of Lovely and Dahlquist (1975) regardless of the employment of the non-smooth tumbling frequency. However, a key argument was that the geometrical factor associated with the random motility coefficient was less dependent on the explicit form of the tumbling frequency function than on whether the function was smooth. In fact, substituting the linear expansion of *any* smooth function for the tumbling frequency should lead to the same result of 2/3.

The accuracy of the theoretical derivations was further verified from numerical examples by finite element solutions. We also studied a case in which chemical gradients were allowed to vary with time and location. We found that our model expressions for μ and V_c based on the modified one-dimensional tumbling frequencies could still be used in such a case and gave almost identical predictions of the bulk concentration profiles to those obtained from the finite element solutions. Thus, the applicability of our model, not limited by the restriction of small chemical gradients, can be confidently extended to a larger variety of situations in which chemical gradients of arbitrary magnitudes decay with time.

When chemotactic bacteria obeyed the biphasic tumbling behavior as described in this paper, our theoretical derivations, based on the consideration of bacterial three-dimensional motion, correctly described such macroscopic transport behaviors, which were confirmed via numerical solutions. Therefore, they are also appropriate to be used in the interpretation of bacterial transport process from experimental data that result from three-dimensional random motion.

Finally, in this work, we concentrated on one uniform turn angle probability density function, $W(\alpha) = 1/2$. This is because the employment of the biphasic tumbling frequency results in piecewise integrations according to each phase of the tumbling frequency. The point at which two adjacent phases are joint is non-smooth. Consequently, explicit forms for $W(\alpha)$ must be given and

universal conclusions cannot be established. It is obvious that if a multi-phase tumbling frequency was used, the integration will be divided into more pieces and yield a more difficult analysis. At present for such a biphasic tumbling behavior, we are unable to analytically verify whether an extension to other functions of $W(\alpha)$ that include nonzero directional persistence still yields $p_r = (1 - \langle \cos\alpha \rangle)/2$ as expected. We plan to verify this hypothesis by employing both numerical and analytical analyses in the near future.

Acknowledgements

This research is supported by a grant from the IBM Environmental Research Program. However, any opinions, findings, and conclusions or recommendations expressed in this material are those of the authors and do not reflect the views of the IBM Corporation.

Notation

a	chemoattractant concentration, mM
$c(z, t)$	bacterial bulk densities, cells/cm^3
D_a	diffusivity of attractants, cm^2/s
$J_z(z, t)$	bacterial net flux in the z direction, cells/s/cm^2
K_d	receptor/ligand dissociation constant, mM
$K(\theta'; \theta)$	the reduced global turning probability density function, dimensionless
L	z-dimension of the computational domain, cm
$n(z, \theta, t)$	bacterial angular number densities as functions of t, z, and θ, cells/cm^3
$n^{\pm}(z, t)$	bacterial subpopulation densities in positive/negative z directions, cells/cm^3
n_0, n_1, n_s	dimensionless perturbation expansion coefficients in cell angular density solution, dimensionless
N_b	chemical-bound receptors per bacterium, receptors/cell
p_0	bacterial basal tumbling frequency, 1/s
p_t	bacterial tumbling frequency, 1/s
$\tilde{p}_t^{\pm}$	bacterial one-dimensional mean tumbling frequencies, 1/s
p_r	one-dimensional reversal probability due to tumbling, dimensionless
$\mathbf{r}$	location vector, cm
R_t	total receptors per cell, receptors/cell
$\hat{s}$	unit vector of the swimming direction, dimensionless
$\hat{s}^*$	representation of $\hat{s}$ in local coordinates, dimensionless
s	one-dimensional swimming speed in Segel's model, cm/s
t	time, s
t_0	initial time, s
t_s	SFDC off-set time, s
v	bacterial swimming speed in three dimensions, cm/s
$v_{1D}^{\pm}$	one-dimensional convective velocities, cm/s
V_c	chemotactic velocity, cm/s
$V_{c,0}$	the leading term of the dimensionless chemotactic velocity, dimensionless
$W(\alpha)$	local turn angle probability density function, dimensionless

Greek letters

α	turn angle between two bacterial consecutive running vectors, deg
α_1, α_2	integration limits defined by Eq. (13), deg
Γ	dimensionless temporal chemical gradient, dimensionless
∇	gradient operator, 1/cm
Δt	discrete time step, s
θ	polar angle of the swimming direction with respect to the z-axis, deg
θ_0	dividing polar angle at which $\Gamma + \xi\cos\theta_0 = 0$, deg
$\kappa(\hat{s}'; \hat{s})$	global turning probability density function as a function of $\hat{s}'$ and $\hat{s}$, dimensionless
$\mathcal{K}$	ratio of the expansion coefficients n_0 to n_s, dimensionless
μ	bacterial diffusion coefficient (random motility coefficient), cm^2/s
μ_0	zeroth-order term of the dimensionless random motility coefficient, dimensionless
μ_1	first-order term of the dimensionless random motility coefficient, dimensionless
ν	scaling factor between chemical stimuli and tumbling responses, s/receptor
ξ	dimensionless spatial chemical gradient, dimensionless
ϕ	azimuthal angle relative to the global z axis, deg
ϕ^*	azimuthal angle relative to the local running vector, deg
ϕ_0^*	azimuthal angle at which the resulting running polar angle is θ_0, deg
χ_0	chemotactic sensitivity coefficient, cm^2/s

Superscripts and subscripts

$^+$	positive moving quantities
$^-$	negative moving quantities
$\langle\rangle$	mean average of ensembles

Appendix. Derivation of regional integral

The specific integral with respect to α over $[\alpha_1, \alpha_2]$ in Eq. (19) can be split into three smaller ones:

$$\int_{\alpha_1}^{\alpha_2} \sin\alpha \begin{bmatrix} \pi(-\Gamma - \xi\cos\alpha\cos\theta') \\ +\phi_0^*(\Gamma + \xi\cos\alpha\cos\theta') \\ -\xi\sin\alpha\sin\theta'\sin\phi_0^* \end{bmatrix} \mathrm{d}\alpha$$

$$= \underbrace{\int_{\alpha_1}^{\alpha_2} -\pi(\Gamma + \xi\cos\alpha\cos\theta')\sin\alpha\,\mathrm{d}\alpha}_{Q_1}$$

$$+ \underbrace{\int_{\alpha_1}^{\alpha_2} \phi_0^*(\Gamma + \xi\cos\alpha\cos\theta')\sin\alpha\,\mathrm{d}\alpha}_{Q_2}$$

$$+ \underbrace{\xi\sin\theta'\int_{\alpha_1}^{\alpha_2} -\sin\phi_0^*\sin^2\alpha\,\mathrm{d}\alpha}_{Q_3}. \tag{A1}$$

The first integral follows directly, and we evaluate the third integral Q_3 now. First, one can express $\sin\phi_0^*$ in terms of α. From Eq. (16) one has, after expanding and rearranging, the following expression:

$$\sin\phi_0^* = \frac{\sqrt{\sin^2\theta'\sin^2\theta_0 - (\cos\alpha - \cos\theta'\cos\theta_0)^2}}{\sin\theta'\sin\alpha}. \tag{A2}$$

Substituting $\sin\phi_0^*$ into Q_3 gives

$$Q_3 = \xi\int_{k_2+k_1}^{k_2-k_1} \sqrt{k_1^2 - (\gamma - k_2)^2}\,\mathrm{d}\gamma$$

$$= -\frac{\xi}{2}\pi(\sin\theta'\sin\theta_0)^2. \tag{A3}$$

Here we have set $k_1 = \sin\theta'\sin\theta_0$, $k_2 = \cos\theta'\cos\theta_0$, and $\gamma = \cos\alpha$. From the definitions of α_1 and α_2, $\cos\alpha_1 = k_2 + k_1$ and $\cos\alpha_2 = k_2 - k_1$.

The second integral Q_2 in Eq. (A1) is separated into two parts to simplify the derivations:

$$Q_2 = \underbrace{\Gamma\int_{\alpha_1}^{\alpha_2} \phi_0^*\sin\alpha\,\mathrm{d}\alpha}_{Q_{2,1}} + \underbrace{\xi\cos\theta'\int_{\alpha_1}^{\alpha_2} \phi_0^*\sin\alpha\cos\alpha\,\mathrm{d}\alpha}_{Q_{2,2}}. \tag{A4}$$

Performing integration by parts, $Q_{2,1}$ becomes

$$Q_{2,1} = \Gamma\left\{-\phi_0^*(\alpha)\cos\alpha|_{\alpha_1}^{\alpha_2} + \int_{\cos\alpha_1}^{\cos\alpha_2} \cos\alpha\,\frac{\partial\phi_0^*(\alpha)}{\partial\cos\alpha}\,\mathrm{d}\cos\alpha\right\}. \tag{A5}$$

Still, we used the symbol γ to represent $\cos\alpha$ and set $k_1 = \sin\theta'\sin\theta_0$ and $k_2 = \cos\theta'\cos\theta_0$. Upon utilizing Eq. (16), the integral at the right-hand side of Eq. (A5) becomes

$$\int_{\cos\alpha_1}^{\cos\alpha_2} \gamma\frac{\partial\phi_0^*}{\partial\gamma}\,\mathrm{d}\gamma$$

$$= \cos\theta_0 \underbrace{\int_{k_2+k_1}^{k_2-k_1} \frac{\gamma^2}{(1-\gamma^2)\sqrt{k_1^2 - (\gamma - k_2)^2}}\,\mathrm{d}\gamma}_{B_1}$$

$$- \cos\theta' \underbrace{\int_{k_2+k_1}^{k_2-k_1} \frac{\gamma}{(1-\gamma^2)\sqrt{k_1^2 - (\gamma - k_2)^2}}\,\mathrm{d}u.}_{B_2} \tag{A6}$$

Before analytically integrating both integrals in Eq. (A6), we performed a change of variables. Call the first integral term in Eq. (A6) B_1 and define the new variables $p = \gamma/k_1$, $t = 1/k_1$, and $r = k_2/k_1$. One derives

$$B_1 = \int\left[\frac{-1}{\sqrt{1-(p-r)^2}} + \frac{t^2}{(t^2-p^2)\sqrt{1-(p-r)^2}}\right]\mathrm{d}p$$

$$= \pi + \int\frac{t^2}{(t^2-p^2)\sqrt{1-(p-r)^2}}\,\mathrm{d}p. \tag{A7}$$

Rearrange the last integral on the right-hand side of Eq. (A7) to be

$$\int\frac{t^2}{(t^2-p^2)\sqrt{1-(p-r)^2}}\,\mathrm{d}p$$

$$= \frac{t}{2}\left\{\int\frac{(t-p)[1-(p-r)^2]}{(t-p)^2[1-(p-r)^2]^{3/2}}\,\mathrm{d}p + \int\frac{(t+p)[1-(p-r)^2]}{(t+p)^2[1-(p-r)^2]^{3/2}}\,\mathrm{d}p\right\}. \tag{A8}$$

Introduce the new variables x and y defined by

$$x = \frac{(t-r)(p-r)-1}{\sqrt{1-(p-r)^2}} \text{ and } y = \frac{(t+r)(p-r)+1}{\sqrt{1-(p-r)^2}} \tag{A9}$$

and the new variables $a = \sqrt{(t-r)^2 - 1}$ and $b = \sqrt{(t+r)^2 - 1}$. Then Eq. (A8), after substituting in suitable integration limits, is simplified and Eq. (A7) becomes

$$B_1 = \pi - \frac{\pi}{2}\left\{\frac{1}{|\cos\theta' - \cos\theta_0|} + \frac{1}{|\cos\theta' + \cos\theta_0|}\right\}. \tag{A10}$$

Similarly, we call the second integral in Eq. (A6) B_2 and rearrange it in terms of the variables t, r, and p, followed by multiplication and expansion of the integrand in the same manner as was done previously in Eq. (A8). It can be found that B_2 is identical to Eq. (A8) except for the

sign of the last term. Judging from Eq. (A10), one can also derive that

$$B_2 = -\frac{\pi}{2}\left\{\frac{1}{|\cos\theta' - \cos\theta_0|} - \frac{1}{|\cos\theta' + \cos\theta_0|}\right\}. \quad \text{(A11)}$$

Organizing the above results for B_1 and B_2 and substituting into Eq. (A5) yields

$$Q_{2,1} = \Gamma\left\{-\phi_0^*(\alpha)\cos\alpha|_{\alpha_1}^{\alpha_2} + \pi\left[\cos\theta_0 + \frac{1}{2}\frac{\cos\theta' - \cos\theta_0}{|\cos\theta' - \cos\theta_0|} - \frac{1}{2}\frac{\cos\theta' + \cos\theta_0}{|\cos\theta' + \cos\theta_0|}\right]\right\}. \quad \text{(A12)}$$

Using a similar method, the other integral $Q_{2,2}$ is integrated by parts and can be found to be

$$Q_{2,2} = \frac{\xi\cos\theta'}{2}\left\{\phi_0^*(\alpha)\sin^2\alpha|_{\alpha_1}^{\alpha_2} - \pi\cos\theta'\sin^2\theta_0\right\} \quad \text{(A13)}$$

where $\gamma = \cos\alpha$, and k_1 and k_2 be defined as before.

To further simplify Q_2, one needs to consider all possible conditions that can happen. Examining the relative locations of θ' and θ_0 in all classified conditions indicated in Fig. 3, we should have the following boundary conditions for ϕ_0^*:

$\phi_0^*(\alpha_1) = \pi,\ \phi_0^*(\alpha_2) = \pi$ for conditions 1(a), (b)

$\phi_0^*(\alpha_1) = 0,\ \phi_0^*(\alpha_2) = \pi$ for conditions 2(a), (c)

$\phi_0^*(\alpha_1) = \pi,\ \phi_0^*(\alpha_2) = 0$ for conditions 2(b), (d)

$\phi_0^*(\alpha_1) = 0,\ \phi_0^*(\alpha_2) = 0$ for conditions 3(a), (b).

Eventually, Q_2 becomes

$$Q_2 = \begin{cases} \pi\Gamma\{-\cos\alpha|_{\alpha_1}^{\alpha_2} + \cos\theta_0 - 1\} + \xi\cos\theta'\dfrac{\pi}{2}\{\sin^2\alpha|_{\alpha_1}^{\alpha_2} - \cos\theta'\sin^2\theta_0\} \\ \qquad\qquad \text{conditions 1(a), (b)} \\ \pi\Gamma\{-\cos\alpha_2 + \cos\theta_0\} + \xi\cos\theta'\dfrac{\pi}{2}\{\sin^2\alpha_2 - \cos\theta'\sin^2\theta_0\} \\ \qquad\qquad \text{conditions 2(a) + 3(a)} \\ \pi\Gamma\{\cos\alpha_1 + \cos\theta_0\} + \xi\cos\theta'\dfrac{\pi}{2}\{-\sin^2\alpha_1 - \cos\theta'\sin^2\theta_0\} \\ \qquad\qquad \text{conditions 2(b) + 3(b)} \\ \pi\Gamma\{\cos\theta_0 + 1\} + \xi\cos\theta'\dfrac{\pi}{2}\{-\cos\theta'\sin^2\theta_0\} \\ \qquad\qquad \text{conditions 4(a), (b).} \end{cases} \quad \text{(A14)}$$

Combining Eq. (A14) with the results of Q_1, Q_3, we can arrive at the final conclusion,

$$\frac{1}{2\pi}\int_{\alpha_1}^{\alpha_2}\sin\alpha\begin{bmatrix}\pi(-\Gamma - \xi\cos\alpha\cos\theta') \\ +\phi_0^*(\Gamma + \xi\cos\alpha\cos\theta') \\ -\xi\sin\alpha\sin\theta'\sin\phi_0^*\end{bmatrix}\mathrm{d}\alpha$$

$$= \begin{cases} \dfrac{\Gamma}{2}(\cos\theta_0 - 1) - \dfrac{\xi}{4}\sin^2\theta_0 & \text{conditions 1(a), (b)} \\ \dfrac{\Gamma}{2}(\cos\theta_0 - \cos\alpha_1) - \dfrac{\xi}{4}\sin^2\theta_0 + \dfrac{\xi}{4}\cos\theta'\sin^2\alpha_1 & \text{conditions 2(a), (c)} \\ \dfrac{\Gamma}{2}(\cos\theta_0 + \cos\alpha_2) - \dfrac{\xi}{4}\sin^2\theta_0 - \dfrac{\xi}{4}\cos\theta'\sin^2\alpha_2 & \text{conditions 2(b), (d)} \\ \dfrac{\Gamma}{2}(\cos\alpha|_{\alpha_1}^{\alpha_2} + \cos\theta_0 + 1) - \dfrac{\xi}{4}\sin^2\theta_0 - \dfrac{\xi}{4}\cos\theta'\sin^2\alpha|_{\alpha_1}^{\alpha_2} & \text{conditions 3(a), (b).} \end{cases} \quad \text{(A15)}$$

References

Alt, W. (1980). Biased random walk models for chemotaxis and related diffusion approximations. *J. Math. Biol.*, *9*, 147–177.

Berg, H.C., & Brown, D.A. (1972). Chemotaxis in *Escherichia coli* analyzed by three-dimensional tracking. *Nature*, *239*, 500–504.

Berg, H.C. (1988). A physicist looks at bacterial chemotaxis. *Cold Spring Harbor Symposia on Quantitative Biology*, (Vol. *LIII*, pp. 1–9).

Berg, H.C. (1993). Random walks in biology (expanded ed.) Princeton: *Princeton University Press.*

Brosilow, B.J., Ford, R.M., Sarman, S., & Cummings, P.T. (1996). Numerical solution of transport equations for bacterial chemotaxis: Effect of discretization of directional motion. *SIAM J. Appl. Math.*, *56*, 1639–1663.

Chen, K.C., Ford, R.M., & Cummings, P.T. (1999). Perturbation expansion of Alt's cell balance equations reduces to Segel's one-dimensional equations for shallow chemoattractant gradients. *SIAM J. Appl. Math. 59*, 35–57.

Chen. K.C. (1997). Transport theory of motile bacterial migration in aqueous phase and small capillaries. Ph.D. dissertation, University of Virginia.

Duffy, K.J., & Ford, R.M. (1997). Turn angle and run time distribution characterize swimming behavior for *Pseudomonas putida*. *J. Bacteriol.*, *179*, 1428–1430.

Ford, R.M., & Cummings, P.T. (1992). On the relationship between cell balance equations for chemotactic cell populations. *SIAM J. Appl. Math.*, *52*, 1426–1441.

Ford, R.M., Phillips, B.R., Quinn, J.A., & Lauffenburger, D.A. (1991). Measurement of bacterial random motility and chemotaxis coefficients. I. Stopped-flow diffusion chamber assay, *Biotechnol. Bioengng*, *37*, 647–660.

Ford, R.M., & Lauffenburger, D.A. (1991). Measurement of bacterial random motility and chemotaxis coefficients. II. Application of single cell-based mathematical model. *Biotechnol. Bioengng*, *37*, 661–672.

Frymier, P.D., Ford, R.M., & Cummings, P.T. (1994). Analysis of bacterial migration: I. Numerical solution of balance equation. *A.I.Ch.E. J.*, *40*, 704–715.

Koster, L.G., Gazi, E., & Seider, W.D. (1993). Finite elements for near-singular systems: Application to bacterial chemotaxis. *Comput. Chem. Engng*, *17*, 485–503.

Lapidus, I.R., & Schiller, R. (1976). Model for the chemotactic response of a bacterial population. *Biophys. J.*, *16*, 779–789.

Lovely, P.S., Dahlquist, F.W. (1975). Statistical measures of bacterial motility and chemotaxis. *J. Theor. Biol. 50*, 477–496.

Macnab, R.M., & Koshland, D.E. (1972). The gradient-sensing mechanism in bacterial chemotaxis. *Proc. Natl. Acad. Sci. U.S.A.*, *69*, 2509–2512.

Madsen, E.L. (1991). Determination *In Situ* biodegradation: facts and challenges, *Environ. Sci. Technol.*, *25*, 1662–1673.

Othmer, H.G., Dunbar, S.R., & Alt, W. (1988). Models of dispersal in biological systems. *J. Math. Biol.*, *26*, 263–298.

Phillips, B.R., Quinn, J.A., & Goldfine, H. (1994). Random motility of swimming bacteria: single cells compared to cell populations. *A.I.Ch.E. J.*, *40* 334–348.

Rivero, M.A., Tranquillo, R.T., Buettner, H.M., & Lauffenburger, D.A. (1989). Transport models for chemotactic cell populations based on individual cell behavior. *Chem. Engng Sci.*, *44*, 2881–2897.

Rivero-Hudec, M.A., & Lauffenburger, D.A. (1986). Quantification of bacterial chemotaxis by measurement of model parameters using the capillary assay. *Biotechnol. Bioengng 28*, 1178–1190.

Schnitzer, M.J. (1993). Theory of continuum random walks and application to chemotaxis. *Phys. Rev.* E, *48*, 2553–2568.

Segel, L.A. (1977). A theoretical study of receptor mechanisms in bacterial chemotaxis. *SIAM J. Appl. Math.*, *32*, 653–665.

Segel, L.A. (1976). Incorporation of receptor kinetics into a model for bacterial chemotaxis. *J. Theoret. Biol.*, *57*, 23–42.

Spudich, J.L., & Koshland, D.E. (1975). Quantitation of the sensory response in bacterial chemotaxis. *Proc. Nat. Acad., USA*, *72*, 710–713.

Staffeld, P.O., Douglas, D.A., & Quinn, J.A. (1987). Mathematical analysis of cell transport phenomena: bacterial chemotaxis in the capillary assay. *Chem. Engng Commun.*, *58*, 339–351.

Widman, M.T., Emerson, D., Chiu, C.C., & Worden, R.M. (1997). Modeling microbial chemotaxis in a diffusion gradient chamber. *Biotechnol Bioengng 55*, 191–205.

Wilson, J.T., Leach, L.E., Henson, M.H., & Jones, J.N. (1986). *In Situ* biodegradation as a ground water remediation technique. *Ground Water Monitoring Rev.*, *6*, 56–64.